Chapter 2
Colorimetric Nanoprobes

Abstract The development of highly sensitive, cost-effective, miniature nanoparticle-based colorimetric nanoprobes attracted great attention in recent years. Depending on their excellent performance in environmental and biological analysis, colorimetric nanoprobes have been widely used for sensing a wide range of analytes/targets, such as metallic cations, anions, small organic molecules, oligonucleotides, proteins, cancer cells, etc. In this chapter, we first introduce the optical absorption properties of nanomaterial, mainly focusing on the noble metal nanomaterials, such as sphere gold nanoparticles, gold nanorods, and silver nanoparticles. Then we discuss the colorimetric sensing strategies for ions, small molecules, oligonucleotides, and protein detection and cellular analysis, highlighting some of their technical challenges and the new trends by means of a set of selected recent applications.

Keywords Noble metal nanomaterials · Optical nanoprobes · Gold nanoparticles · Silver nanoparticles · Colorimetric sensing

2.1 Optical Absorption Properties of Nanomaterials

As materials are reduced in size from the bulk to the nanoscale, they begin to exhibit new and unusual chemical and physical properties [1, 2]. Noble metallic nanostructures have attracted enormous scientific interest because of their unique size or shape dependent properties, including large optical field enhancements resulting in the strong scattering and absorption of light [3, 4]. Low-dimensional structures such as nanoparticles and nanostructured materials have excellent properties, such as quantum confinement of electrons and holes, surface effects, and geometrical confinement of phonons [4, 5].

In the last two decades, the interest in gold and silver metallic particles has dramatically increased, mostly because of their unique optical and electronic properties [3–8]. These unique properties are mainly due to the collective

L. Chen et al., *Novel Optical Nanoprobes for Chemical and Biological Analysis*, SpringerBriefs in Molecular Science, DOI: 10.1007/978-3-662-43624-0_2,

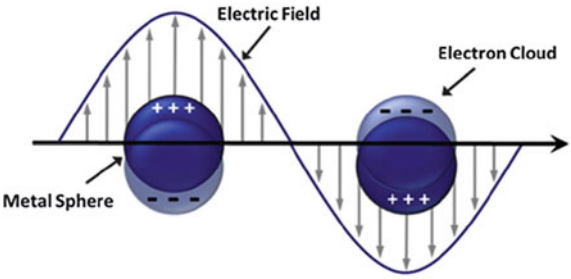

Fig. 2.1 Schematic diagrams illustrating localized surface plasmon resonance. Adapted with permission from Ref. [9]. Copyright 2014, Royal Society of Chemistry

excitation of the conduction band electrons known as the surface plasmon resonance (SPR). The surface plasmon is a specific type of plasma oscillation occurring at lower energies than bulk plasmon, which happens when light is coupled to the coherent oscillation of free electrons at the surface of a conductor. This type of oscillation at resonant conditions is called the SPR. When the SPR is localized to a volume with dimensions smaller than the wavelength of incident light, it is called localized surface plasmon resonance (LSPR) [9].

When the particle dimensions are too small to support a propagating wave, light will interact with metal particles smaller than the wavelength of incident light to generate a LSPR (Fig. 2.1). The confinement of a surface plasmon to a small volume results in an oscillating electromagnetic field that resides very close to the particle surface, extending only nanometers into the dielectric environment [10]. Therefore, LSPR can generate much higher local field enhancements (100–10,000 times the incident field) comparing to those of SPP (10–100 times the incident field) [11]. The LSPR frequency can be tuned by changing the material composition, size, shape, and dielectric environment [12], which for gold, silver, and copper lies in the visible region [13].

Small spherical particles have a single, sharp absorption band due to the excitation of what is called a dipole plasmon resonance, where the entire charge distribution of the particle oscillates at the frequency of the incident electric field as illustrated in Fig. 2.1. For gold nanoparticles (Au NPs), the resonance condition is satisfied at visible wavelengths, which attributing for its intense color. Au NPs in the 10 nm size range have a strong absorption maximum around 520 nm in water due to their LSPR [9]. As shown in Fig. 2.2, Au NPs of different sizes present various color with different characteristic absorption bands.

Anisotropic particles can arise various LSPR modes. Nanorods are the quintessential demonstration of how optical properties are dependent on the dimensions (or shape) of a particle. The dipole plasmon resonance of a solution of nanorods is typically split between transverse and longitudinal dipole resonances due to the different dimensions along the width and length of the particles (Fig. 2.3A) [15]. The two bands positions depend on both the aspect ratio and the absolute dimensions of the particles [15]. The resonance at the longer wavelength (the longitudinal plasmon resonance) is associated with oscillations along the length of the nanorod, while the resonance at the shorter wavelength (the

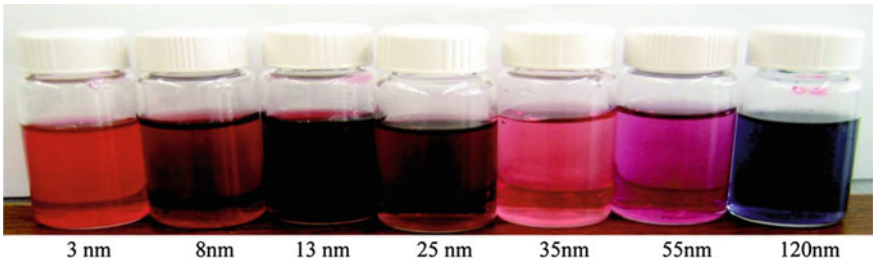

Fig. 2.2 Photograph showing gold nanoparticles of different sizes. Reprinted with permission from Ref. [14]. Copyright 2009, Wiley-VCH

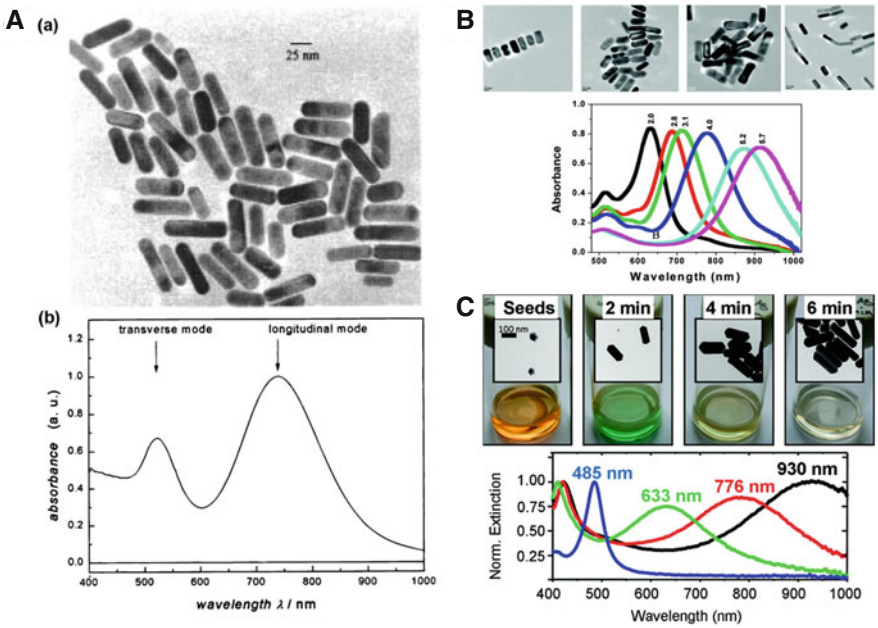

Fig. 2.3 **A** (a) TEM image of Au nanorods and (b) corresponding extinction spectrum. Due to the anisotropy of the particles, the dipole plasmon resonance is split into a transverse plasmon absorption at 525 nm and a longitudinal plasmon absorption at 740 nm. Adapted with permission from Ref. [15]. Copyright 1999, American Chemical Society. **B** TEM image of gold nanorods of average aspect ratios (σ) $\approx$ 2.0, 2.8, 4.0, and 5.2; Extinction profile of Au nanorods with aspect ratios varying from 2.0 to 5.7. The strong long wavelength band in the near-infrared region (λLPR = 600–950 nm) is due to the longitudinal oscillation of the conduction band electrons. The short wavelength peak ($\lambda \approx$ 520 nm) is from the nanorods' transverse plasmon mode. Reprinted with permission from Refs. [2, 18]. Copyright 2008, Wiley VCH. **C** Representative silver nanorod samples are shown as photographs and TEM images together with the corresponding ensemble extinction spectra (*bottom*). The samples correspond to Ag-seeds and Ag-nanorods grown with 2, 4, and 6 min of heating time (from *left* to *right*). Their plasmon peak increases from 485 to 633, 776, and 930 nm. Reprinted with permission from Ref. [17]. Copyright 2011, American Chemical Society

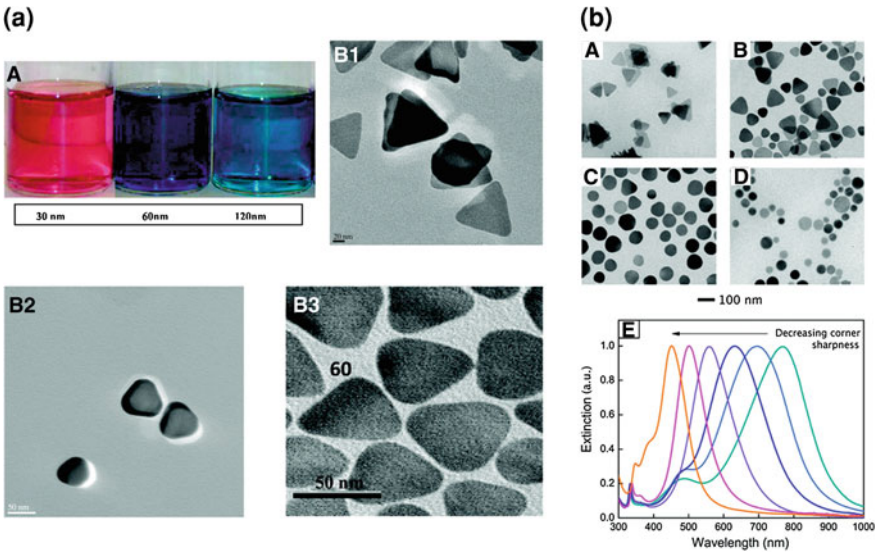

Fig. 2.4 **a** (A) Photographic images. (B1–B3) TEM pictures of silver nanoprisms of different sizes (30, 60, and 120 nm edge length). Reprinted with permission from Ref. [21]. Copyright 2009, Elsevier. **b** (A–D) TEM images of Ag *triangular nanoplates* with decreasing corner sharpness. The sharp cornered *triangular plates* in (A) were rounded until the particles had a *circular disk shape* (D). (E) The decreasing corner sharpness is correlated with a blue-shift in the extinction spectra of the nanoparticles in solution. Reproduced with permission from Ref. [20]. Copyright 2010, Wiley

transverse plasmon resonance) is associated with oscillations along the width of the nanorods [15, 16]. The LSPR of nanorods depend strongly on the aspect ratio. For example, Au NRs of different aspect ratio show various positions of two bands (Fig. 2.3B), the longer wavelengths exhibit red shift with the increasing of aspect ratio. The silver nanorods present the similar optical properties (seen in Fig. 2.3C). The absorption bands changed with the increasing of the aspect ratio [17].

The certain anisotropic particles can have extinction spectra that are greatly influenced by higher ordered resonances as evidenced by the in-plane and out-of-plane quadrupolar resonances observed for samples of silver triangular nanoprisms [19, 20]. As shown in Fig. 2.4a, with the increasing of edge length, silver nanoparisms showed red to blue color change. The decreasing of corner sharpness is correlated with a blue shift in the extinction spectra of silver nanoprisms (Fig. 2.4b).

The various compositions of nanoparticles could cause the change of SPR frequency with visible changes to the color of a colloid [22, 23]. As shown in Fig. 2.5A, the addition of sulfide ions into the Au@Ag core–shell nanocubes generated stable Au@Ag/Ag_2S core–shell nanoparticles at room temperature, and the plasmon extinction maximum shifts to the longer wavelength covering the entire visible range of 500–750 nm with full-color tuning [24]. The silver-coated

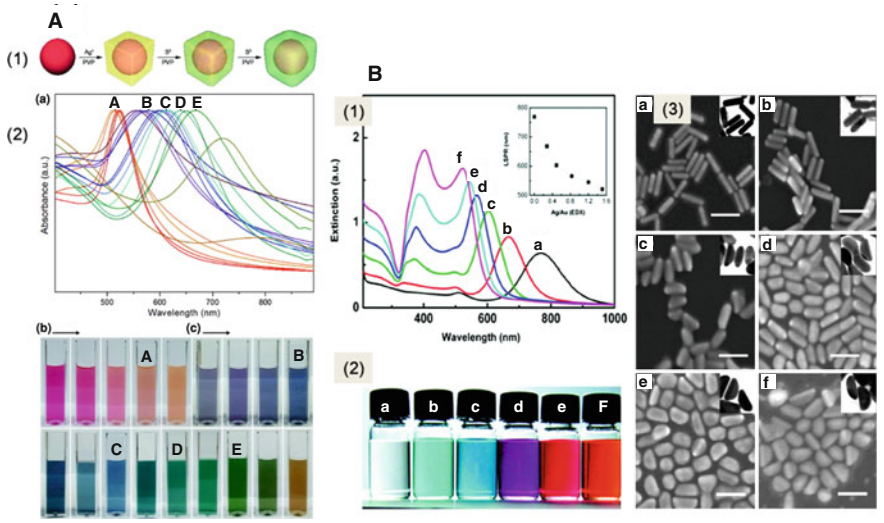

Fig. 2.5 **A** (1) Synthesis of Au@Ag/Ag_2S core–shell nanoparticles surface plasmon resonance shifts of Au seeds, Au@Ag core–shell nanocubes, and Au@Ag/Ag_2S nanoparticles. (2) (a) UV-vis absorption spectra. Photographs of the aqueous dispersions of (b) Au seeds and Au@Ag core–shell nanocubes, and (c) Au@Ag/Ag_2S nanoparticles. The representative samples are referred to as A (*orange*), B (*dark blue*), C (*blue*), D (*bluish green*), and E (*green*). Reprinted with permission from Ref. [24]. Copyright 2012, American Chemical Society. **B** (1) UV-vis extinction spectra of (a) Au NRs and (b–f) the Au@Ag core/shell nanocrystals with Ag/Au molar ratios. The *inset* in panel A shows the relationship between the longitudinal SPR position and the Ag/Au molar ratio. (2) Photographs of nanocrystal dispersions corresponding to the *curves* in panel 1. (3) SEM images of (a) Au NRs and (b–f) Au@Ag core/shell nanocrystals with Ag/Au molar ratios of 0.28, 0.49, 0.83, 1.20, and 1.51 measured by EDX. The *scale bar* is 60 nm. *Insets* are corresponding STEM images with the same *scale bar*. Reproduced with permission from Ref. [23]. Copyright 2012, American Chemical Society

gold nanorods from homogeneous coating to anisotropic coating also exhibit peak position shift [23]. As shown in Fig. 2.5B, with increasing overall amount of the deposited Ag, the longitudinal SPR band blue shifts obviously, while the transverse SPR band blue shifts slightly and is finally smeared out by the former.

Furthermore, the SPR frequency is sensitive to the proximity of other nanoparticles. When two or more discrete plasmonic materials are in close proximity to one another (on the order of nanometers), their oscillating electric fields can interact to yield new resonances and the surface plasmons will be coupled [25]. For instance, the aggregation of Au NPs results in significant red-shifting (from $\sim$520 to $\sim$650 nm for 13 nm Au NPs) and broadening in the surface plasmon band, changing the solution color from red to blue due to the interparticle plasmon coupling [3]. This visibly apparent phenomenon has made Au NPs an attractive candidate for colorimetric sensors [7–26].

Colorimetric assay is that the molecular recognition event can be transformed into color change, which can be easily observed by the naked eye. Depending on

their size, shape, degree of aggregation, and sensitive surface, novel metallic nanoparticles can appear abundant colors and emit bright resonance light scattering of various wavelengths. Therefore, spherical nanoparticles and nonspherical structures (e.g., prisms, rods, cubes) with unique shape-dependent properties can be extensively explored as colorimetric probes with the help of recognition moiety for sensing a wide range of analytes/targets, such as metallic cations, nucleic acids, proteins, cells, etc. [5, 7]. Owing to the excellent optical properties, gold and silver nanostructures are most attractive for optical applications.

2.2 Colorimetric Sensing Strategies

Nanomaterial-based colorimetric methods are commonly based on the change of optical properties due to assemblies (or aggregations), morphology transition, and the surface chemical reaction, accompany by distinct color change. Two key components are essentially necessary in a colorimetric assay and affect the performance in selectivity, sensitivity, response time, and signal-to-noise ratio. One is the recognition moiety that provides a selective/specific response to the analyte, which relates to a wide range of organic or biological ligands/reactions. The other is the transducer moiety that translates detecting behavior into an eye-sensitive color change in the visible range of 390–750 nm [27]. Based on the behavior of nanoparticles, colorimetric sensing strategies can be summarized as two types: one is based on the analyte-induced aggregation of nanoparticles, called aggregation-based method. The other mainly uses the morphology transition and the surface chemical reaction of single particle, which is called single particle morphology-based method.

2.2.1 Aggregation-Based Methods

The aggregation of noble metal nanoparticles (Au/Ag) of appropriate sizes induces interparticle surface plasmon coupling, resulting in a visible color change. For instance, the aggregation of Au NPs ($d > 3.5$ nm) induces interparticle surface plasmon coupling, resulting in a visible color change from red to blue at nanomolar concentrations [7, 28, 29]. The color change during nanoparticle aggregation provides a practical platform for absorption-based colorimetric sensing of any target analyte that directly or indirectly triggers the nanoparticles aggregation.

Aggregation-based colorimetric nanoprobes have been widely explored [5]. Generally, nanoparticles are modified different types of functional decorators such as oligonucleotides, aptamer, functional molecules (Fig. 2.6), the presence of target analyte can induces the aggregation by specific interaction with functional ligands, resulting in two types of aggregation: crosslinking aggregation and non-crosslinking aggregation.

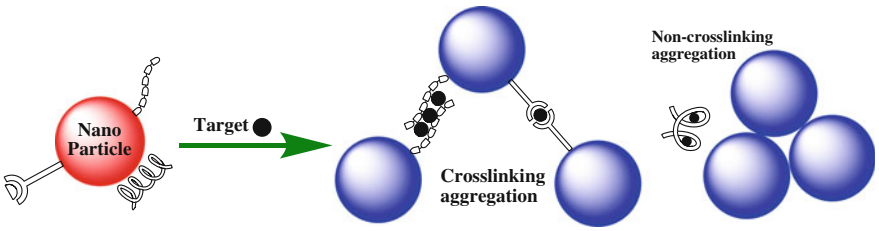

Fig. 2.6 Schematic illustration of aggregation-based colorimetric nanoprobe

Crosslinking aggregation-based colorimetric sensing methods generally require the incorporation of chelating agents onto the nanoparticle surface. The presence of target analyte induces the nanoparticle aggregation by forming multidentate interparticle complexes with the chelating ligand (Fig. 2.6). Thiol is one of the main functional groups for tethering to the surface of nanoparticles due to the strong Au–S or Ag–S bond. Therefore, mercapto derivatives of ligands become preferred decorators for a nanoprobe system. The incentives of crosslinking aggregation in nanoparticle-based colorimetric methods involve chelate reaction, chemical interaction, electrostatic interaction, base paring, hydrogen-bonding recognition, and so on.

For instance, Chen et al. developed an Au NP-based colorimetric assay for mercury ions (Hg^{2+}) detection using the coordination reaction between thymine (T) and Hg^{2+} [30]. The synthesized N-1-(2-mercaptoethyl) thymine can be easily coupled to the surface of Au NPs through Au–S bond. The presence of Hg^{2+} could effectively induce the aggregation of Au NPs by forming a T–Hg–T complex with strong affinity owing to the active N site, resulting in a significant color change from red to blue (Fig. 2.7a). This is a typical crosslinking aggregation-based strategy using the chelate reaction between ligands and metal ions. Jiang's group reported a method for the detection of copper ions (Cu^{2+}) by azide-and terminal alkyne-functionalized Au NPs in aqueous solutions using click chemistry [31]. When Cu^{2+} and the reductant (sodium ascorbate) were both introduced to the mixture of azide- and alkyne- functionalized Au NPs, Cu (I) could catalyze 1, 3-dipolar cyclo-addition of alkynes and azides on the surface of functionalized Au NPs, resulting in the aggregation of Au NPs (Fig. 2.7b). Cao et al. explored a simple and visual approach to colorimetric detection of nuclease activity using the electrostatic interaction between positively charged Au NPs and negatively charged DNA [32]. The polyanionic ssDNA used as the S1 nuclease substrate could induce the aggregation of (+) Au NPs, which can be observed via the color change from red to blue. During the enzymatic reaction of S1 nuclease, ssDNA is degraded to smaller fragments, which cannot induce the color change (Fig. 2.7c). Thus, electrostatic interaction-induced aggregation of Au NP-based colorimetric method was achieved. DNA-base paring meditated Au NPs assembly was demonstrated by Mirkin's group [33]. In this method, two thiolated ssDNA modified Au NP probes were fabricated for colorimetric detection of target oligonucleotides (Fig. 2.7d). Upon the addition of target, Au NPs aggregation was trigged with

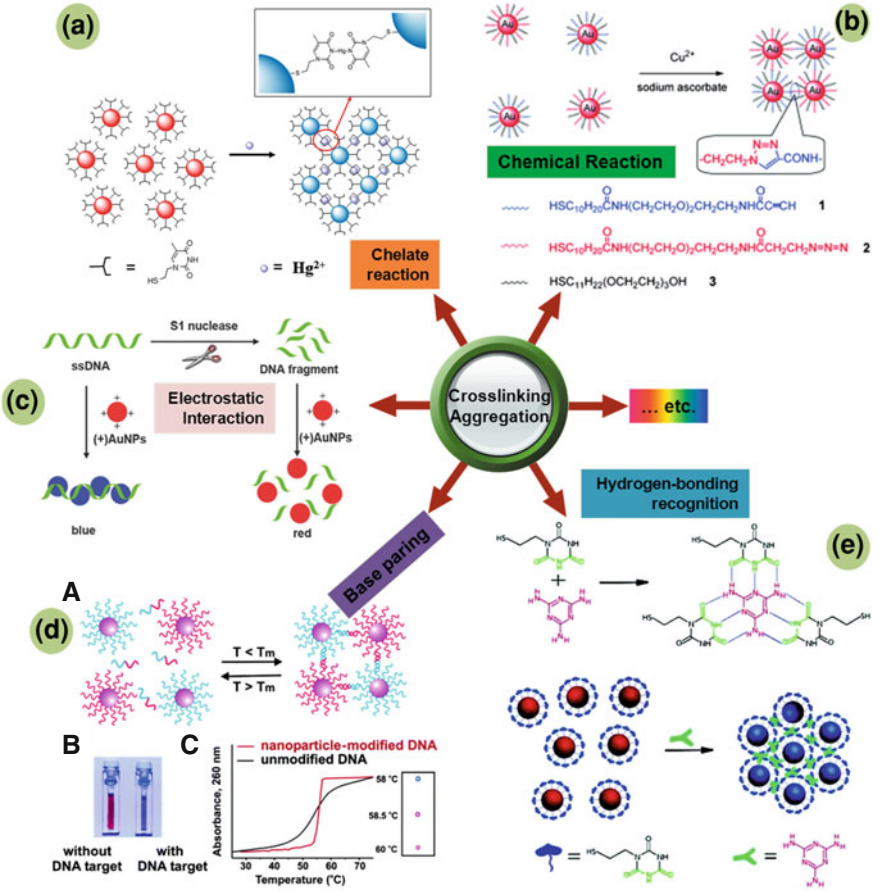

Fig. 2.7 Illustration of the crosslinking aggregation-based colorimetric nanoprobes. **a** Schematic mechanism of T–S–Au NPs sensing Hg^{2+} in aqueous solutions based on the Hg^{2+}-induced aggregation of gold nanoparticles. Reprinted with permission from Ref. [30]. Copyright 2011, Royal Society of Chemistry. **b** The detection of Cu^{2+} ions using click chemistry between two types of gold NPs, each modified with thiols terminated in an alkyne (1) or an azide (2) functional group. Reprinted with permission from Ref. [31]. Copyright 2008, Wiley. **c** Colorimetric assay of nuclease activity based on the color change of the positively charged gold nanoparticles ((+)AuNPs). Charge interaction between (+) AuNPs and polyanionic ssDNA leads to the aggregation of the AuNPs, which can be observed via the color change from *red* to *blue*. During the enzymatic reaction of S1 nuclease, ssDNA is degraded to smaller fragments, and the smaller fragments cannot induce the color change. Reprinted with permission from Ref. [32]. Copyright 2011, Royal Society of Chemistry. **d** In the presence of complementary target DNA, oligonucleotide-functionalized gold nanoparticles will aggregate (A), resulting in a change of solution color from *red* to *blue* (B). The aggregation process can be monitored using UV-vis spectroscopy or simply by spotting the solution on a silica support (C). Reprinted with permission from Ref. [35]. Copyright 2005, American Chemical Society. **e** Hydrogen-bonding recognition between melamine and cyanuric acid derivative. Colorimetric detection of melamine using the MTT-stabilized gold nanoparticles. Reprinted with permission from Ref. [34]. Copyright 2008, American Chemical Society

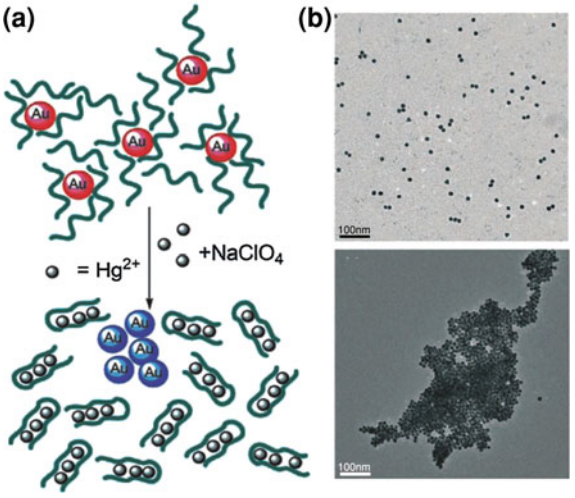

Fig. 2.8 **a** Schematic representation of Hg^{2+} stimulated aggregation of AuNPs and **b** TEM images of non-aggregated AuNPs stabilized by ssDNA in the presence $NaClO_4$ and the aggregated Au NPs after addition of Hg^{2+}. Reproduced with permission from Ref. [36]. Copyright 2008, Wiley

concomitant color change as a result of hybridization of the DNA strand. Highly specific base-pairing of DNA strands coupled with the intense absorptivity of Au NPs enables the subpicomolar quantitative colorimetric detection of oligonucleotides. Lu's group developed a hydrogen-bonding recognition-induced color change of Au NPs for visual detection of melamine in raw milk and infant formula [34]. Upon exposure of the synthesized 1-(2-mercaptoethyl)-1, 3, 5-triazinane-2, 4, 6-trione (MTT)-stabilized Au NPs to melamine, hydrogen-bonding recognition between melamine and MTT resulted in the aggregation of Au NPs, and the wine red color was accordingly changed to a blue color (Fig. 2.7e).

Another type of aggregation-based method relies on noncrosslinking aggregation of nanoparticles in different modes. Generally, free specific ligands are treated with nanoparticles through weaker interaction. Macroscopic changes of nanoparticles were attributed to the stronger interaction between ligands and target analyte, and following release of ligands from the surface of nanoparticles. The system became so destabilized that nanoparticles aggregated. For instance, Willner and coworkers fabricated a simple, fast, and wide-range system for the detection of Hg^{2+} using T rich-nucleic acid [36]. After treating Au NPs (13 nm) with ssDNA, $NaClO_4$ (100 mM) was added into the solution to maintain a high level of salinity. Under this condition, red color with an absorption band at 520 nm was observed before addition of Hg^{2+}, indicating good dispersion of the nanoparticles. Upon addition of Hg^{2+} the solution turned blue, induced by aggregation of Au NPs, which was detected by the naked eye and also confirmed by a red shift and broadened peak in the UV-vis spectrum. Macroscopic changes were attributed to the formation of the nucleic acid duplex-folded complex with the help of Hg^{2+}, and following release of ssDNA from Au NPs. As a result, the system became so destabilized that Au NPs aggregated (Fig. 2.8).

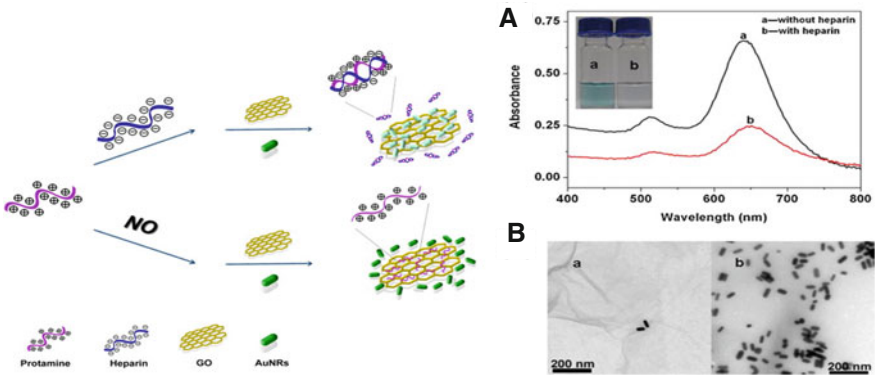

Fig. 2.9 Schematic illustration of GO quenching the color of Au NRs sensing heparin based on the self-assembly of CTAB-stabilized Au NRs on the surface of GO. **A** Absorption spectra and **B** TEM images of Au NRs in the GO/protamine mixed solutions in the absence (a) and presence (b) of heparin (0.24 μg/mL). *Inset* of part **A**: Photographic images of the corresponding colorimetric response (*scale bars* 200 nm). Reprinted with permission from Ref. [37]. Copyright 2011, Elsevier

A novel label-free colorimetric strategy was developed for ultrasensitive detection of heparin by using the super color quenching capacity of graphene oxide (GO) by Fu et al. [37]. Hexadecyltrimethylammonium bromide (CTAB)-stabilized Au NRs could easily self-assemble onto the surface of GO through electrostatic interaction, resulting in the decrease of the SPR absorption and consequent color quenching change of Au NRs from deep to light. Polycationic protamine was used as a medium for disturbing the electrostatic interaction between Au NRs and GO, as shown in Fig. 2.9. The Au NRs were prevented from adsorbing onto the surface of GO because of the stronger interaction between protamine and GO, showing a native color of Au NRs. On the contrary, in the presence of heparin, which was more easily to combine with protamine, the Au NRs could self-assemble onto the surface of GO, resulting in the native color disappearing of Au NRs. The amounts of self-assembled Au NRs were proportional to the concentration of heparin, and thereby the changes in the SPR absorption and color had been used to monitor heparin levels. A good linearity was obtained in a range of 0.02–0.28 μg/mL, and a limit of detection (LOD) was 5 ng/mL.

Redox formed metal coating on the surface of nanoparticles is an excellent analytical strategy for noncrosslinking-aggregation based colorimetric assay. Lou et al. developed a "blue-to-red" colorimetric method for determination of mercury ions (Hg^{2+}) and silver ions (Ag^{+}) based on stabilization of Au NPs by redox formed metal coating in the presence of ascorbic acid (AA) [38]. In this method, Au NPs were first stabilized by Tween 20 in phosphate buffer solution with high ionic strength. In a target ion-free system, the addition of N-acetyl-L-cysteine resulted in the aggregation of Tween 20 stabilized Au NPs for mercapto-ligand self-assembled on the surface of Au NPs, which induced the Au NPs to be

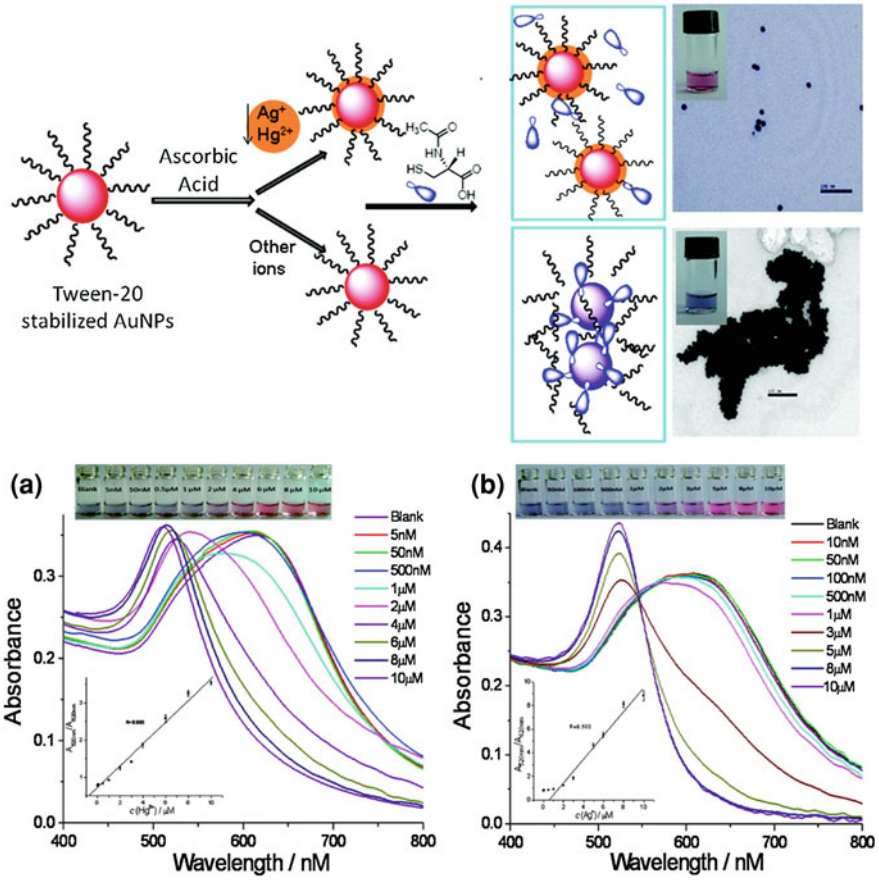

Fig. 2.10 Illustration of colorimetric sensing mechanism based on redox reaction modulated surface chemistry of Au NPs; TEM image of aggregated Au NPs in Hg^{2+}-free PBS solution and the monodispersed Au NPs Obtained after Addition of 10 μM Hg^{2+}. Digital photographs, absorption spectra, and plots of $A_{520\ nm}/A_{620\ nm}$ versus the concentration (*inset*) in 50 mM PBS (pH 7.2) containing Tween 20-Au NPs, 1 mM AA, and 0.1 M NaCl (0.01 M EDTA) upon addition of **A** 0–10 μM Hg^{2+} and **B** Ag^{+}. The incubation time was 3 min. The error bars represented standard deviations based on three independent measurements. Reprinted with permission from Ref. [38]. Copyright 2011, American Chemical Society

unstable. This would lead to a color change from red to blue. By contrast, in an aqueous solution with Hg^{2+} or Ag^{+}, the ions could be reduced with the aid of AA to form Hg–Au alloy or Ag coating on the surface of Au NPs. This metal coating blocked mercapto-ligand assembly and Au NPs kept monodispersed after addition of N-acetyl-L-cysteine, exhibiting a red color, as shown in Fig. 2.10. This method could selectively detect Hg^{2+} and Ag^{+} as low as 5 and 10 nM with a linear range of 0.5–10 μM for Hg^{2+} and 1.0–8.0 μM for Ag^{+}, respectively.

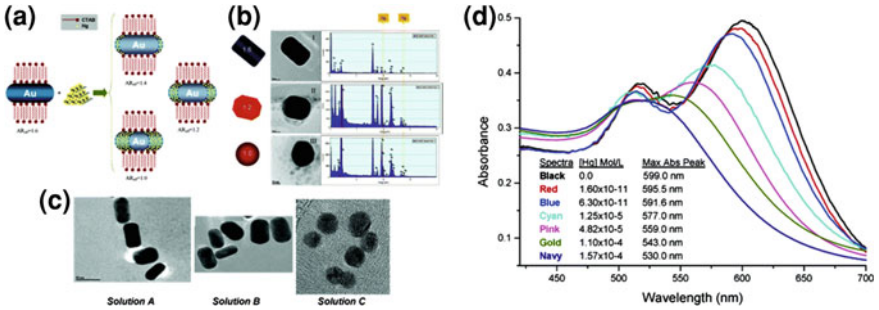

Fig. 2.11 Schematic diagram showing the amalgamation of Hg with Au nanorods. **B** TEM and EDX analysis of Au nanorods in the absence and the presence of Hg. I = no Hg; II = 1.25×10^{-5} M and III = 1.57×10^{-4} M Hg^{2+}. All solutions were prepared in 1.67×10^{-3} mol/L $NaBH_4$. **C** TEM analysis of multiple Au nanorods in the absence and the presence of Hg. Sol A, no Hg; Sol B, 1.25×10^{-5} M Hg; Sol C, 1.57×10^{-5} M Hg^{2+}. All solutions were prepared in 1.67×10^{-3} mol/L $NaBH_4$. UV-visible absorption spectra showing the spectral shift at several Hg (II) concentrations. The concentration range between 1.6×10^{-11} and 6.3×10^{-11} M shows the spectra within the linear dynamic range of the calibration curve. The remaining spectra show the overlapping between the longitudinal and transversal absorption bands at higher Hg (II) concentrations. Reproduced with permission from Ref. [41]. Copyright 2006, American Chemical Society

2.2.2 Single Particle Morphology-Based Methods

The color-tunable behavior of nanoparticles depends on the size and shape enables nanomaterials an attractive candidate for the colorimetric nanoprobes. Many kinds of nanomaterials involve gold nanoparticles (spheres, rods), silver-coated gold nanoparticles, silver nanoprisms have been used for colorimetric probes [39, 40], relying on the analyte-induced morphology transition, and the surface chemical reaction of single particle, calling the single particle morphology-based methods.

Campiglia et al. provided a direct way to determine mercury using the morphology change of Au NRs resulted from the well-known amalgamation process that occurs between mercury and gold [41]. With the addition of Hg^{2+} and reductant ($NaBH_4$) to the Au NRs solution, chemical reactions involved in the amalgamation of mercury and gold gradually occurred at the active sites of Au NRs-the tips of nanostructures, that could cause a reduction of effective aspect ratio of the nanorods and a blue shift of the maximum absorption wavelength of the longitudinal mode band (Fig. 2.11).

Lou et al. explored a colorimetric, label-free, and nonaggregation-based silver-coated gold nanoparticles (Ag/Au NPs) probe for detection of trace Cu^{2+} in aqueous solution, based on the fact that Cu^{2+} can accelerate the leaching rate of Ag/Au NPs by thiosulfate ($S_2O_3^{2-}$) [42]. The leaching of Ag/Au NPs would lead to dramatic decrease in the SPR absorption as the size of Ag/Au NPs decreased (Fig. 2.12). This colorimetric strategy based on size-dependence of nanoparticles during their leaching process provided a highly sensitive (1.0 nM) and selective

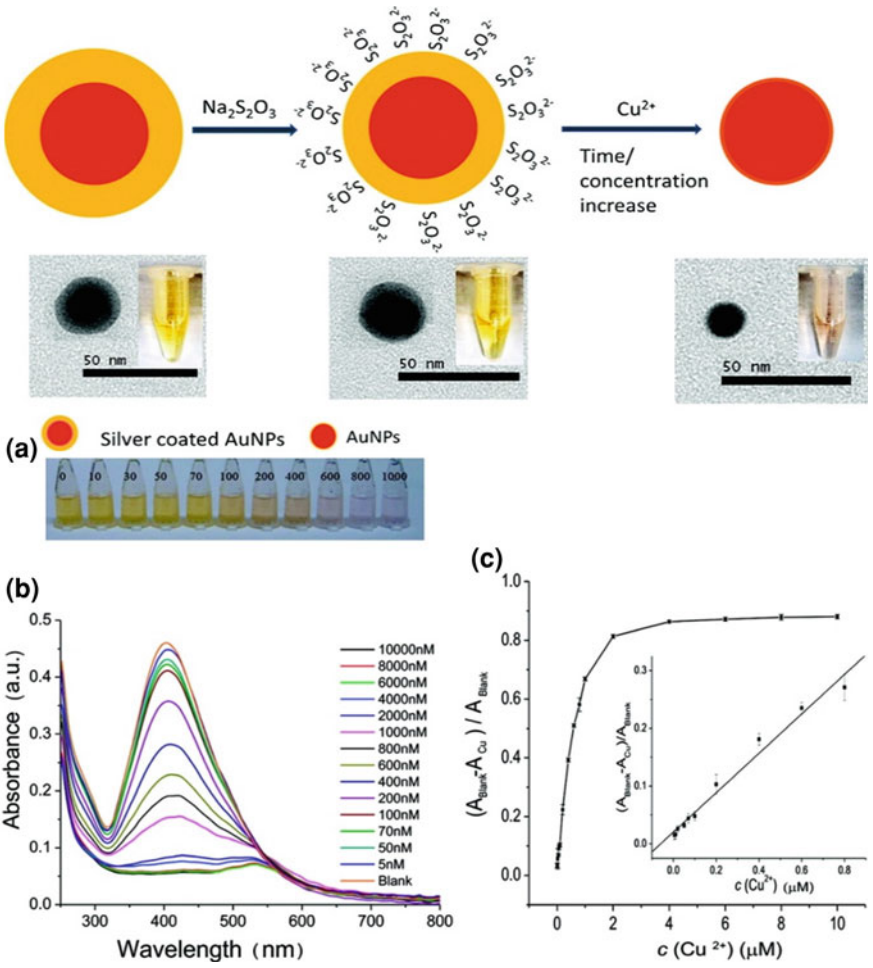

Fig. 2.12 Schematic representation of the sensing mechanism of the $S_2O_3^{2-}$–Ag/AuNPs for the colorimetric detection of Cu^{2+} based on catalytic leaching of Ag-coated Au NPs. **A** Photographs and **B** absorption responses of the $S_2O_3^{2-}$–Ag/AuNP solution addition of Cu^{2+}, and **C** plot of $(A_{blank}-A_{Cu})/A_{blank}$ (at 405 nm) values versus Cu^{2+} concentration. *Inset* the enlarged portion of the plot in the Cu^{2+} concentration range of 5–800 nM; the regression equation is $(A_{blank}-A_{Cu})/A_{blank} = 0.0202 + 0.341c$ (μM) ($r = 0.991$). Reprinted with permission from Ref. [42]. Copyright 2011, American Chemical Society

detection toward Cu^{2+}, with a wide linear detection range (5–800 nM) over nearly three orders of magnitude. Wang et al. also developed a silver-coated gold nanorod-based Cu^{2+} probe by the same reaction principle [43]. A sensitive colorimetric sensing method for AA was also developed via target-induced silver overcoating using mesoporous silica-coated Au NRs [44].

Yang's group designed a homogeneous system consisting of Ag nanoprisms and glucose oxidase (GOx) for simple, sensitive, and low-cost colorimetric sensing of

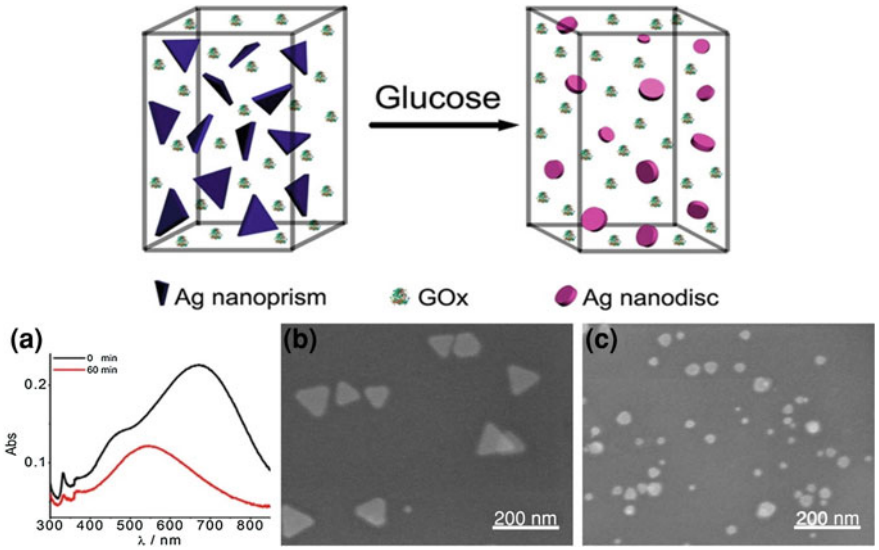

Fig. 2.13 Schematic illustration of the (Ag nanoprism)-GOx homogenous system for colorimetric sensing of Glucose. SPR absorption spectra (**A**) and SEM images of the Ag nanoprisms before (**B**) and after (**C**) incubation with GOx and glucose (100 μ M) for 60 min. Reprinted with permission from Ref. [45]. Copyright 2013, American Chemical Society

glucose in serum [45]. In this study, the unmodified Ag nanoprisms and GOx are first mixed with each other. Glucose is then added in the homogeneous mixture. Finally, the nanoplates are etched from triangle to round by H_2O_2 produced by the enzymatic oxidation (Fig. 2.13), which leads to a more than 120 nm blue shift of the SPR absorption band of the Ag nanoplates. This large wavelength shift can be used not only for visual detection (from blue to mauve) of glucose by naked eyes but also for reliable and convenient glucose quantification in the range from 2.0×10^{-7} to 1.0×10^{-4} M. The detection limit is as low as 2.0×10^{-7} M, because the used Ag nanoprisms possess not only highly reactive edges/tips but also strongly tip sharpness and aspect ratio dependent SPR absorption. Owing to ultrahigh sensitivity, only 10–20 μL of serum is enough for a one-time determination.

2.3 Applications

2.3.1 Ionic Detection

Colorimetric nanoprobes have been widely developed for ionic detection in environmental and biological analysis, including alkali and alkaline earth metal ions, heavy metal ions, anions. These colorimetric sensing methods were mainly fabricated using novel metal nanoparticles. Table 2.1 summarized the key characteristics of colorimetric nanoprobes for ionic detection.

Table 2.1 Key characteristic of colorimetric nanoprobes for target analysis

Target/Analyte	Nanomaterial	Detection linear range	Sensing strategy	References
Metal ions				
Hg^{2+}	Au NPs	0.1–2.0 μM	Hg^{2+} will coordinate selectively to the bases that make up a T–T mismatch	[46]
	Au NPs	250–500 nM	Hg^{2+} induce the aggregation of mercaptopropionic acid-modified Au NPs	[47]
	Au NRs	0.016 nM–157 μM	Hg^{2+} was reduced by sodium borohydride to form amalgamation and cause a reduction of the aspect ratio of AuNRs	[41]
	Au NPs	0.5–50 μM	Hg^{2+} induces the aggregation of DNA/AuNPs	[48]
	Au NPs	10–300 nM	Hg^{2+} induces the non-crosslinking aggregation of T_{33}-DNA/Au NPs	[49]
	Au NPs	5–1,000 nM	Hg^{2+} bridged crosslinking aggregation of N-1-(2-mercaptoethy) thymine modified Au NPs	[30]
	Au NPs	0.2–6.0 μM	Hg^{2+} induces the non-crosslinking aggregation of mononucleotides-stabilized Au NPs	[50]
	Au NPs	2–12 μM	Hg^{2+} inhibits the thymine-induced aggregation of Au NPs	[51]
	Ag NPs	2–1,000 nM	Catalytic reduction property of Ag NPs	[52]
	Silver nanoprisms	10–500 nM	Hg^{2+} indirectly induce the morphology transition of silver nanoprisms	[53]
Hg^{2+}, Ag^{+}	Au NPs	200–800 nM for Hg^{2+} 400–1,000 nM for Ag^{+}	Hg^{2+} and Ag^{+} were reduced by citrate to form Hg–Au alloys and Ag on the surface of the Au NPs	[54]
	Au NPs	0.5–10 μM for Hg^{2+} 1.0–8.0 μM for Ag^{+}	Blue-to-red colorimetric sensing for Hg^{2+} and Ag^{+} via redox-regulated surface chemistry of Au NPs	[38]
Hg^{2+}, Pb^{2+}, Cu^{2+}	Au NPs	4–28 μM	The interaction between protein-functionalized Au NPs and metal ions	[55]

(continued)

Table 2.1 (continued)

Target/Analyte	Nanomaterial	Detection linear range	Sensing strategy	References
Pb^{2+}	Au NPs	2.5 Nm–10 μM	Pb^{2+} ions accelerate the leaching rate of Au NPs by thiosulfate ($S_2O_3^{2-}$) and 2-mercaptoethanol (2-ME)	[39]
	Au NPs	3 nM–1 μM (pH 7.2) 120 nM–20 μM (pH 5.5)	AuNPs aggregate in the absence of lead but remain dispersed in the presence of lead by the addition of DNAzyme and NaCl	[56]
	Au NPs (5–8 nm)	0.1–50 μM	Pb^{2+} induce the aggregation of glutathione-stabilized Au NPs	[57]
As^{3+}	Au NPs	0–450 ppt	As^{3+} induces the crosslinking aggregation of GSH/DTT/Cys-modified Au NPs	[58]
Cd^{2+}	Au NPs	0.2–1.7 μM	Cd^{2+}-induced the aggregation of 6-mercaptonicotinic acid and L-Cysteine co-functionalized Au NPs	[59]
Cr^{3+}	Au NPs	0.1–1.0 μM	N-benzyl-4-(pyridin-4-ylmethyl)aniline modified Au NPs aggregated in the presence of Cr^{3+}	[60]
Cr (VI)	Au NRs	0.1–20 μM	Selective etching of Au NRs at tips	[61]
Co^{2+}	Au NPs	0.1–0.7 μM	Co^{2+} induce aggregation of thiosulfate stabilized gold nanoparticles in the presence of ethylenediamine	[62]
Cu^{2+}	Au NPs	50–500 μM	Assay for Cu^{2+} by the aggregation of azide and alkyne functionalized Au NPs as a result of the Cu(I)-catalyzed conjugation	[31]
	Au@Ag NPs	5–800 nM	Cu^{2+} accelerate leaching of silver-coated gold nanoparticles	[42]
	Ag NPs	3.2–512 ppb	Cu^{2+} can interact with dopamine during the synthesis of silver/dopamine nanoparticles	[63]
	Au NRs	10–300 nM	Cu^{2+} accelerate decomposition of H_2O_2 using Au NRs	[64]
	Au@Ag NRs	3–1,000 nM	Cu^{2+} accelerate the leaching of silver-coated gold nanorods	[43]
	Au NRs		Cu^{2+} accelerate the etching of Au NRs by dissolved oxygen in the presence of NH_3–NH_4Cl	[65]

(continued)

Table 2.1 (continued)

Target/Analyte	Nanomaterial	Detection linear range	Sensing strategy	References
Fe^{3+}	Au NPs	10–60 μM	Fe^{3+} induce the aggregation of pyrophosphate functionalized Au NPs	[66]
K^+	Au NPs	7.6–140 μM	15-crown-5 moieties functionalized Au NPs	[67]
	Au NPs	6.25–112 μM	15-crown-5-$CH_2O(CH_2)_{12}SH$ functionalized Au NPs	[68]
Ca^{2+}	Au NPs	0.1–1.6 mM	Cytidine triphosphate stabilized gold nanoparticles	[69]
	Au NPs	1.9–20 μM	1-thiohexyl carboxylic acid and 1-thiohexyl β-D-lactopyranoside in bi-ligand functionalized AuNPs	[70]
Eu^{3+}	Au NPs	50–496 nM	Crosslinking aggregation of tetramethylmalonamide (TMMA) functionalized Au NPs	[71]
Anions				
NO_2^-	Au NPs	20–35 μM	Nitrite coupled Griess reaction between aniline Au NPs and naphthalene Au NPs	[72]
	Au NRs	5.2–60 μM	Nitrite trigger the non-crosslinking aggregation of 4-aminothiophenol modified Au NRs	[73]
	Au NRs	1.0–15 μM	Nitrite trigger the etching of Au NRs at the ends	[74]
HCl	Au NPs	500 ~ 5,000 ppm	Nonaggregation-based detection system relies on the ability of chloro species to cause rapid leaching of Au NPs in an aqueous dispersion containing a strong oxidizing agent	[75]
I^-	Au NPs	10–600 nM	Anti-aggregation of Au NPs	[76]
SCN^-	Au NPs	0.2–2 μM	SCN^- induce the non-crosslinking aggregation of Tween 20-stabilized Au NPs	[77]
Small organic molecules				
TNT	Au NPs	0.5 pM–5 nM	TNT-induced the aggregation of cysteamine stabilized Au NPs	[78]
	Au NPs	50–250 μM	TNT trigger the aggregation of *p*-ATP attached Au NPs	[79]

(continued)

Table 2.1 (continued)

Target/Analyte	Nanomaterial	Detection linear range	Sensing strategy	References
Glucose	Ag nanoprism	0.2 ~ 100 μM	Silver nanoprisms are etched from triangle to round by H_2O_2 produced by the enzymatic oxidation	[45]
	Au NPs	10–90 μg/mL	Glucose oxidase immobilized Au NPs aggregate in the presence of glucose	[80]
Dopamine	Au NPs	5–350 nM	Dopamine induces the aggregation of both 4-mercaptophenylboronic acid (MBA) and dithiobis(succinimidylpropionate) (DSP) functionalized the Au NPs	[81]
	Au NPs	0.2–1.1 μM	Hydrogen-bonding recognition induced aggregation of 4-amino-3-hydrazino-5-mercapto-1,2,4-triazol (AHMT) functionalized Au NPs	[82]
Melamine	Au NPs	0–400 nM	Hydrogen-bonding recognition-induced color change of 1-(2-mercaptoethyl)-1,3,5-triazinane-2,4,6-trione (MTT) modified Au NPs	[34]
	Au NPs	0.6–1.6 μM	Melamine can induced the aggregation of Au NPs and results in the color change from wine-red to purple	[83]
Ascorbic acid	Au NPs	4.4 ~ 30 nM	Alkyne–azide click reaction using gold nanoparticles with the addition of Cu^{2+}	[84]
	Mesoporous silica coated Au NRs	0.1–2.5 μM	Tailoring the optical properties of mesoporous silica-coated Au NRs via silver overcoating	[44]
ATP	Au NPs	0.6 ~ 132.7 μM	Au NP-based aptamer target binding readout for ATP assay	[85]
	Au NPs	0.1–1 mM	Adenosine induces assembly of aptazyme functionalized Au NPs	[86]
	Au NPs	0.3–2 mM	Aptamer attached Au NPs	[87]
Cocaine		50–500 μM	Cocaine binding aptamer attached Au NPs	[87]
		2–200 nM	Cocaine can interact with engineered aptamer and induce the aggregation of Au NPs	[88]
Streptomycin	Au NPs	2 nM ~ 1.8 μM	Streptomycin induces the aggregation of MPA-AuNPs based on the electrostatic interaction between streptomycin and MPA	[89]

(continued)

Table 2.1 (continued)

Target/Analyte	Nanomaterial	Detection linear range	Sensing strategy	References
Clenbuterol	Au NPs	0.28–280 nM 280–1,400 nM	Hydrogen-bonding interaction between clenbuterol and melamine result in the aggregation of Au NPs	[90]
Oxytetracycline	Au NPs	1–200 μM	Oxytetracycline bound aptamer and Au NPs aggregate in the presence of salt	[91]
Organophosphate pesticide	Au NPs	2.51–18.7 pM for VX 15.0–52.5 pM for GD 28.2–225 pM for GB 45.2–495 fM for paraoxon	Catalytic reaction of acetylcholine esterase (AChE) and the aggregation of lipoic acid capped AuNPs	[92]
Phthalates	Au NPs	1–10,000 ppm	UTP-modified gold nanoparticles cross-linked by copper(II)	[93]
Cysteine	Au NPs	0.01–100 μM	Self-assembly of cysteine on gold nanoparticles in the presence of copper ions	[94]
Cysteine and glutathione	Au NRs	1.75–3 μM for Cys 7–14 μM for GSH	Cysteine and glutathione induce assembly of Au NRs	[95]
D-Cys	Ag NPs	0.1–20 μM	UTP-capped Ag NPs can be used as an ultrahigh efficiency enantioseparation and detection platform for D-and L-cysteine	[96]
Oligonucleotides				
Single nucleotide polymorphisms	Au NPs	2–80 nM	Single-stranded DNA binding protein–nucleic acids interaction and unmodified Au NPs	[97]
Nucleic acids	Au NPs	2–10 nM	Nonionic morpholino oligos functionalized Au NPs	[98]
Proteins				
Nuclease	Au NPs	0 ~ 30 U/mL	Charge interaction between positively-charged AuNPs and long DNA	[32]

(continued)

Table 2.1 (continued)

Target/Analyte	Nanomaterial	Detection linear range	Sensing strategy	References
Thrombin	Au NPs	2 ~ 167 nM	Aptamer-functionalized Au NPs for the amplified optical detection of thrombin	[99]
Histone-modifying enzymes	Au NPs	1–200 nM	Antibody-mediated assembly of Au NPs decorated with substrate peptides	[100]
Platelet-derived growth factors	Au NPs	2.5–200 nM	Aptamer modified Au NPs aggregate in the presence of target	[101]
Trypsin and inhibitor	Au NPs	1.6–8.0 ng/mL	Using crosslinking/aggregation of Au NPs based on trypsin-catalyzed hydrolysis of Arg6	[102]
Acetylcholinesterase	Au NPs	0 ~ 5.0 mU/mL	AChE could hydrolyze ATC to generate thiocholine, which could induces the aggregation of AuNPs	[103]
DNA methyltransferase/ glycosylase	Au NPs	2–104 U/mL for Dmnt1 1.6–256 U/mL for hOGG1	Covalent capture of target enzymes by activity-based DNA probes which created terminal protection of the DNA probes tethered on AuNPs from degradation by Exo I and III	[104]
Cells				
Ramos cell line	Au NPs	90 ~ 4,000 cells	Au NP-based colorimetric assay for the direct detection of cancerous cells	[105]
Breast cancer SK-BR-3 cell lines	Oval-shaped gold nanoparticle	10 ~ 10^6 cells/mL	Multifunctional (monoclonal anti-HER2/c-erb-2 antibody and S6 RNA aptamer-conjugated) oval-shaped gold-nanoparticle-based nanoconjugate	[106]

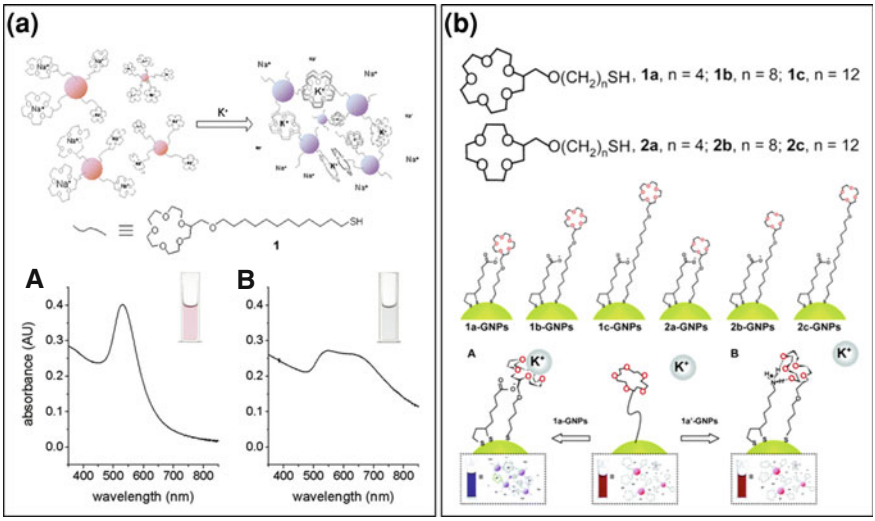

Fig. 2.14 **a** Schematic representation of the K^+-Induced aggregation via sandwich complexation of crown-thiol molecule 1 in a sodium-containing solution. UV-visible spectra and photographs of solutions of 2.5 mM Na^+ + 7.1 nM colloidal gold containing (A) Li^+, Cs^+, NH_4^+, Mg^{2+}, and Ca^{2+}(0.1 mM each) and (B) the above species and 0.1 mM K^+. Reprinted with permission from Ref. [67]. Copyright 2002, American Chemical Society. **b** Structures of crown thiols employed in the modification of Au NPs; Relative positions of the carboxylate and crown moiety for crown thiols with different chain lengths; Proposed structures of the crown moiety preorganized due to the neighboring molecules of (A) thioctic acid and (B) thioctic amine. The cuvettes contain 16.5 nM concentrations of the corresponding Au NPs, 100 μM K^+, and 2.5 mM Na^+. Reprinted with permission from Ref. [68]. Copyright 2005, American Chemical Society

Colorimetric detection for Alkali and alkaline earth metal ions has been investigated using Au NP-based probes. 15-crown-5 moieties functionalized Au NPs have been fabricated for the colorimetric detection of potassium ions (K^+) via formation of a 2:1 sandwich complex between 15-crown-5 moiety and K^+ [67]. This nanoprobe showed highly sensitive and selective colorimetric response toward K^+ even in the presence of physiologically important cations, including Li^+, Cs^+, NH_4^+, Mg^{2+}, Ca^{2+}, and excess Na^+ (Fig. 2.14a). Later, the performance of this probe system was improved by bi-ligand co-functionalized Au NPs with thioctic acid and crown thiols [68]. The rate of K^+ recognition increased from this system has been attributed to a cooperative effect that allows crown moiety to be preorganized by the negatively charged carboxylate moiety of the thioctic acid for K^+ recognition. Utilizing this principle the analogous detection of Na^+ in urine has been achieved by incorporating 12-crown-4 onto the Au NP surface together with the thioctic acid (Fig. 2.14b). In a similar fashion Ca^{2+} has been detected by utilizing 1-thiohexyl carboxylic acid and 1-thiohexyl β-D-lactopyranoside co-functionalized Au NPs [70].

Heavy metal ions such as Hg^{2+}, Pb^{2+}, As^{3+}, and Cd^{2+} have been well-known significant health hazards. Colorimetric nanoprobes for heavy metal ions detection

have been designed using novel metal nanoparticles carrying specific ligands, such as aliphatic acid, aptamer, DNA enzyme. Hupp et al. have reported a simple colorimetric technique for the detection of trace toxic metals such as Pb^{2+}, Cd^{2+}, Hg^{2+} [107]. In this system, the aggregation of 13 nm Au NPs capped with 11-mercaptoundecanoic acid was driven by ion recognition and binding, the color change could be employed for visual sensing of the ions. Chang et al. developed a similar method for Hg^{2+} detection using mercaptopropionic acid-modified Au NPs in the presence of 2, 6-pyridinedicarboxylic acid [47]. For colorimetric Hg^{2+} detection, the specific affinity between thymine (T) and Hg^{2+} has been a considerable recognition moiety. Dependent on T–Hg^{2+}–T coordination chemistry, the colorimetric assay for Hg^{2+} was first developed by the Mirkin's group based on a complementary DNA-Au NP system with designed T–T mismatches [46]. As shown in Fig. 2.15A, two types of nanoparticles aggregated together after the specially designed ssDNA hybridized, causing a red-to-purple color change. After raising the temperature to the melting temperature (T_m), the dsDNA de-hybridized, which made Au NP aggregates dissociate reversibly along with a color change back to red. Among environmentally relevant metal ions, only Hg^{2+} could raise the T_m obviously as shown in Fig. 2.15B. The sharp melting transition enhanced the sensitivity and lowered the LOD visibly to 100 nM (20 ppb) in contrast to organic colorimetric system. Based on the above works, Liu et al. developed a system that was not only selective and sensitive but also practical and convenient for colorimetric detection of Hg^{2+} at room temperature [48]. Introduction of Hg^{2+} into an aqueous solution containing oligonucleotide-tethered gold nanoparticle probes and a linker oligonucleotide with a number of T–T mismatches results in the formation of particle aggregates at room temperature with a concomitant colorimetric response. The high selectivity of this detection system is attributed to Hg^{2+}-mediated formation of T–Hg^{2+}–T base pairs as evidenced by an increase in a sharp melting temperature. This colorimetric assay showed high selectivity toward Hg^{2+} in the presence of other metal ions (Fig. 2.15D).

Thymine molecule derivatives such as thiolated thymine and deoxythymidine triphosphates also have been used as the specific ligands for Hg^{2+} detection in Au NP-based colorimetric probes [30, 50, 51]. Compared with T rich-DNA oligomers, small thymine molecule derivatives seem to be more simple and easier to be combined to the surface of nanoparticles. Yang's group designed a new approach for simple and rapid colorimetric detection of Hg^{2+} based on Hg^{2+} induced aggregation of deoxythymidine triphosphates (dTTPs)-functionalized Au NPs [50]. The dTTPs could protect bare Au NPs from aggregation in the presence of salt ($KClO_4$). With the addition of Hg^{2+}, the dTTPs were desorbed from the Au NPs surface by the interaction of Hg^{2+} with the adsorbed dTTPs by forming T–Hg^{2+}–T complex, thus induced aggregation of Au NPs, resulting in a red to blue–gray color change of Au NPs owing to the interparticle coupled plasmon excitons in the aggregated states (Fig. 2.15E). This method exhibited high sensitivity toward Hg^{2+} with a LOD of 50 nM (Fig. 2.15F). Later, Lou et al. proposed a colorimetric detection method for Hg^{2+} by using anti-aggregation of Au NPs based on the coordination between thymine and Hg^{2+} [51]. In this study, the thymine can

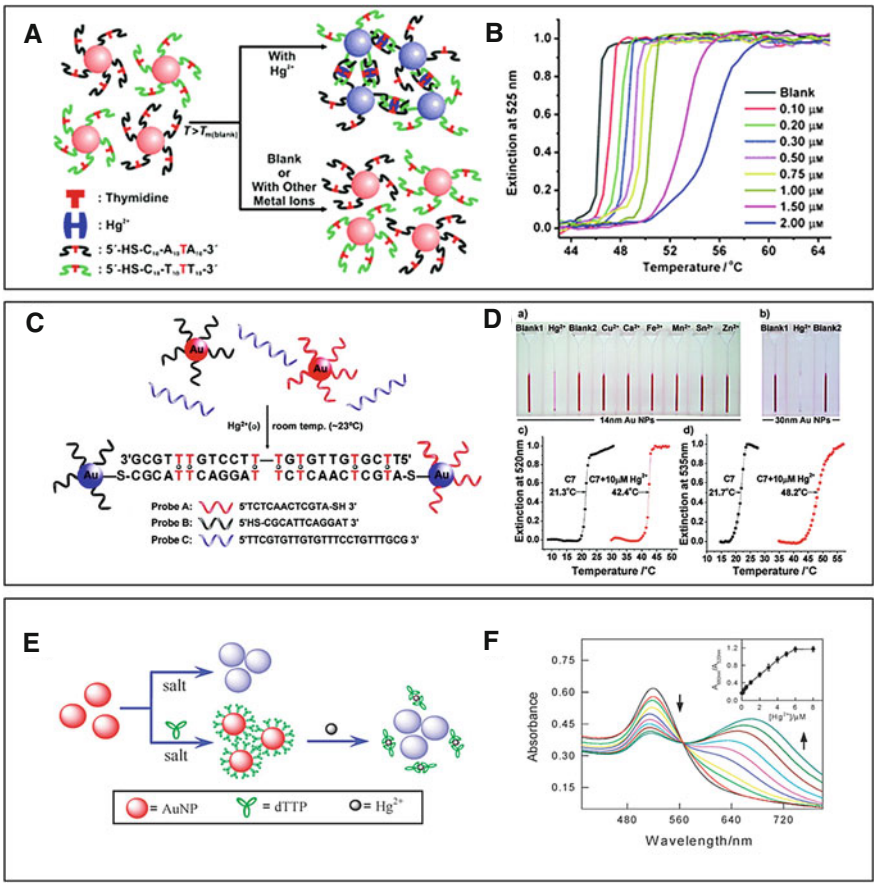

Fig. 2.15 **A** Colorimetric detection of Hg^{2+} using DNA-Au NPs and **B** Normalized melting *curves* of aggregates (probes A and B) with different concentrations of Hg^{2+}. Reproduced with permission from Ref. [46]. Copyright 2007, American Chemical Society. **C** Schematic representation of colorimetric detection of Hg^{2+} using ssDNA-Au NPs and **D** (a) Color response of a 14 nm NP detection system (probes A, B, and C7) in the presence of a selection of metal ions (Hg^{2+}, Cu^{2+}, Ca^{2+}, Fe^{3+}, Mn^{2+}, Sn^{2+}, Zn^{2+}; 10 μM each). Note that Blank1 (probes A, B, and C7 without Hg^{2+}) and Blank2 (probes A and B with Hg^{2+}) were used as control references. (b) Color response of a 30 nm NP detection system under the same conditions. (c, d) Normalized melting *curves* of the solution (containing probe A, B, and C7) with or without Hg^{2+} (10 μM) for the 14 and 30 nm NP systems, respectively. Reproduced with permission from Ref. [48]. Copyright 2008, American Chemical Society. **E** Schematic description of colorimetric sensing of Hg^{2+} based on the dTTPs-stabilized Au NPs absorption spectra changes of T–Au NPs solution in the presence of different concentrations of Hg^{2+}. **F** The *arrows* indicate the signal changes as increases in Hg^{2+} concentrations. *Inset* plot of the value of absorbance ratios, $A_{680\ nm}/A_{520\ nm}$, of T–Au NPs as a function of the concentration of Hg^{2+}. Reproduced with permission from Ref. [50]. Copyright 2011, Royal Society of Chemistry

bind to the Au NPs through Au–N bonds and induce aggregation of Au NPs. In the presence of Hg^{2+}, the thymine was released from the surface of Au NPs via the formation of a thymine-Hg^{2+} coordination complex, leading to the dispersion of Au NPs.

Colorimetric nanoprobes for Pb^{2+} detection have been largely developed by using the size and distance dependent optical properties of nanoparticles [39, 108, 109]. Huang's group designed a colorimetric assay for Pb^{2+} based on the leaching of Au NPs owing to the fact that Pb^{2+} accelerates the leaching rate of Au NPs by thiosulfate ($S_2O_3^{2-}$) and 2-mercaptoethanol (2-ME) [39]. The formation of Pb–Au alloys on the surfaces of the Au NPs in the presence of Pb^{2+} and 2-ME. The formation of Pb–Au alloys accelerated the Au NPs rapidly dissolved into solution, leading to dramatic decreases in the SPR absorption (Fig. 2.16A). The 2-ME/$S_2O_3^{2-}$–Au NP probe is highly sensitive (LOD = 0.5 nM) and selective (by at least 1,000-fold over other metal ions) toward Pb^{2+}, with a linear detection range (2.5 nM–10 μM) over nearly four orders of magnitude.

DNAzymes, a type of DNA-based catalysts, obtained through the combinatorial method systematic evolution of ligands by exponential enrichment (SELEX), can direct assembly of Au NPs. Lu's group have fabricated highly selective Pb^{2+} sensors using DNAzyme-directed assembly of Au NPs [56]. The design of label-free DNAzyme colorimetric Pb^{2+} sensor is based on the 8–17 DNAzyme highly specific for Pb^{2+} composed of a substrate strand extended by eight bases at the 5' end (called (8)17S) and an enzyme strand extended by eight complimentary bases at 3' end (called 17E(8)) (Fig. 2.16B). The 8-base-pair extension allows stable hybridization between the substrate and enzyme strands at ambient temperature, while still allowing release of single stranded DNA (ssDNA) at the other end upon cleavage in the presence of Pb^{2+}. Upon addition of trishydroxymethylaminomethane (Tris) and NaCl to adjust ionic strength, followed by addition of Au NPs, the released ssDNA can be adsorbed onto Au NP and prevent the individual Au NP from forming blue aggregates under high-ionic-strength conditions. In the absence of Pb^{2+} or in the presence of other metal ions, however, no cleavage reaction should occur, and the enzyme–substrate complex can not stabilize Au NPs, resulting in Au NP aggregates. This sensor showed high sensitivity with a detection limit of 3 nM. For simplicity, Su et al. developed a facile, cost-effective colorimetric detection method for Pb^{2+} by using glutathione functionalized Au NPs [57]. The modified Au NPs could be induced to aggregate immediately in the presence of Pb^{2+} with the addition of NaCl (Fig. 2.16C).

Glutathione, dithiothreitol, and cysteine co-functionalized Au NPs have been fabricated for As^{3+} detection (1 ppb) in groundwater [58]. Au NPs modified with 5, 5'-dithiobis (2-nitrobenzoic acid) were also used for the detection of trace levels Cr^{3+} (99.6 ppb) in the presence of 15 other metal ions in aqueous solution [60]. 6-mercaptonicotinic acid and L-cysteine co-functionalized Au NPs were used for colorimetric detection of Cd^{2+} (LOD = 100 nM) [59]. Generally, there is no specific recognition ligand for these metal ions, two or more ligands are used to co-modify Au NPs with synergistic effect in colorimetric assay.

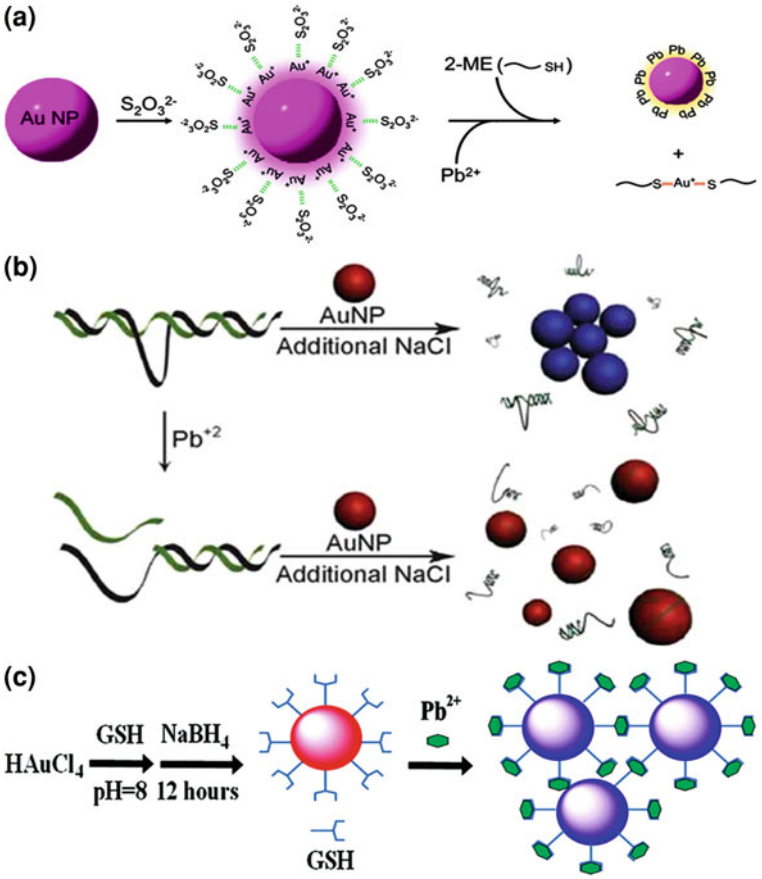

Fig. 2.16 **A** Cartoon representation of the sensing mechanism of the 2-ME/$S_2O_3^{2-}$–Au NP Probe for the detection of Pb^{2+} ions. Reproduced with permission from Ref. [39], Copyright 2009, American Chemical Society. **B** *Left* Secondary structure of the DNAzyme complex, which consists of an enzyme strand (17E(8)) and a substrate strand ((8)17S). After lead-induced cleavage, 10-mer ssDNA is released which can adsorb onto the AuNP surface. *Right* Schematic of the label-free colorimetric sensor. The lead-treated/-untreated complex and NaCl are mixed with AuNPs. The AuNPs aggregate in the absence of lead but remain dispersed in the presence of lead. Reproduced with permission from Ref. [56], Copyright 2008, Wiley. **C** Strategy for the colorimetric detection of Pb^{2+} using GSH-Au NPs Reproduced with permission from Ref. [57], Copyright 2010, American Chemical Society

Hutchison and coworkers have developed a trivalent lanthanide (Ln^{3+}) ion sensor based on tetramethylmalonamide (TMMA) functionalized Au NPs [71]. The presence of Ln^{3+} ions in the Au NP solution initiates Au NP cross-linking and concomitant red to blue color change through the formation of 2:1 TMMA-Ln^{3+} chelating complex. An immediate colorimetric response to the Ln^{3+} ions was detected, with sensitivity down to $\sim$50 nM for Eu^{3+} and Sm^{3+}.

Colorimetric assay also has been explored for anions detection. The Griess reaction where sulfanilamide and naphthylethylenediamine are coupled by nitrite has been used to create colorimetric assay for NO_2^- detection. Mirkin's group designed a colorimetric nitrite sensor with Au NP probes [72]. In the system, two types of Au NPs were used, aniline Au NPs were modified with 5—[1, 2] dithiolan-3-yl-pentanoic acid [2-(4-amino-phenyl)ethyl]amide and co functionalized with hydrophobic (11-mercapto-undecyl)-trimethyl-ammonium (MTA) with molecules to increase their solubility; naphthalene Au NPs were modified with 5—[1, 2] dithiolan-3-yl-pentanoic acid [2-(naphthalene-1-ylamino)et-hyl]amide and MTA. The aniline and naphthalene Au NPs are red when dispersed in aqueous solution. In the presence of NO_2^- under acidic conditions, however, the amine groups on the aniline Au NPs are converted to a diazonium salt, which then couples with the naphthalene Au NPs to form covalently interconnected nanoparticle probes. This reaction causes the formation of crosslinked particle networks which precipitate rapidly, causing the solution to change from red to colorless (Fig. 2.17a). A novel noncrosslinking NO_2^- sensor was developed utilizing 4-aminothiophenol (4-ATP) modified Au NRs [73]. In the presence of nitrite ions, the deamination reaction was induced by heating the 4-ATP modified Au NRs in ethanol solution, resulting in the reduction of the Au NRs surface charge, which led to aggregation and a colorimetric response that was quantitatively correlated to the concentration of nitrite ions (Fig. 2.17b). This simple assay was rapid ($\leq$10 min) and highly sensitive (<1 ppm of nitrite), and it can be used for rapid monitoring of drinking water quality. Zhang et al. developed a simple colorimetric method for sensing of nitrite as low as 4.0 μM by naked eyes [74]. This method is based on etching of Au NRs accompanied by shape changes in aspect ratios (length/width) and a visible color change from bluish green to red and then to colorless with the increase of nitrite (Fig. 2.17c). Colorimetric nanoprobes for other anions such as I, SCN^- also have been investigated with efforts [76, 77].

2.3.2 Detection of Small Organic Molecules

A variety of colorimetric detection methods for small organic molecules such as glucose, adenosine triphosphate (ATP), cocaine, 2, 4, 6-trinitrotoluene (TNT), dopamine, have been developed based on novel metal nanoparticles, as summarized in Table 2.1.

TNT is a leading example of a nitroaromatic explosive with significant detrimental effects on the environment and human health. Mao and coworkers reported a simple and sensitive method for the colorimetric visualization of TNT at picomolar levels by using Au NPs [78]. This method was based on the color change of Au NPs induced by the donor–acceptor (D–A) interaction between TNT and primary amines (Fig. 2.18A). In this system, cysteamine was used both as the primary amine and as the stabilizer for Au NPs. Cysteamine-stabilized AuNPs were well dispersed and the color was wine red. In the presence of TNT, the D–A

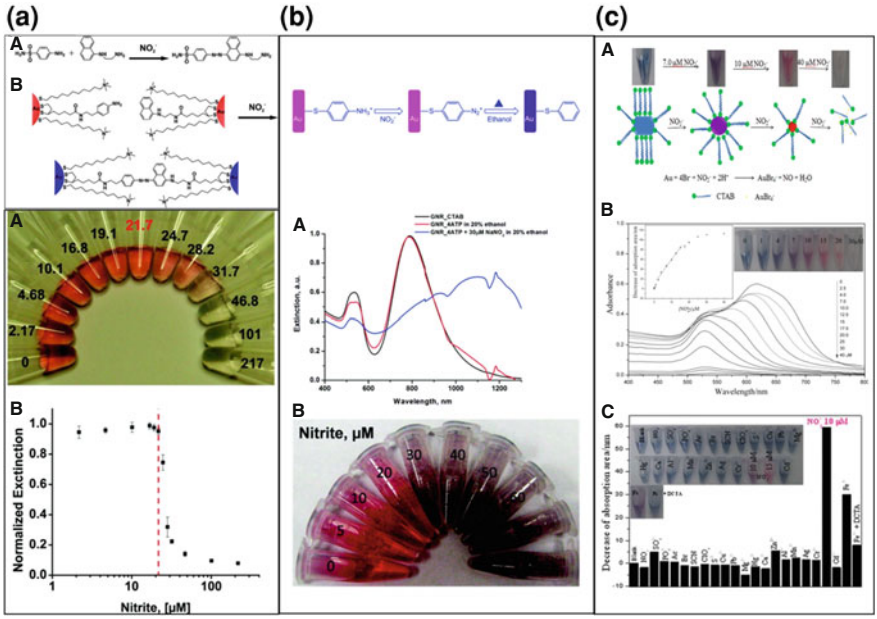

Fig. 2.17 **a** Griess reaction; Colorimetric detection of nitrite with functionalized Au NPs photograph of particle solutions after incubation with various concentrations of nitrite. The nitrite concentrations, in μM, are listed next to the respective solutions. The MCL of nitrite in drinking water (21.7 μM) is highlighted in *red*. (B) Particle solution extinction at 524 nm after incubation as a function of nitrite concentration. The *red dashed line* indicates the nitrite MCL. Reprinted with permission from Ref. [72], Copyright 2009, American Chemical Society. **b** Noncross-linking colorimetric detection of nitrite with 4-ATP modified Au NRs; (A) Absorption spectra of CTAB covered Au NRs (*black*), Au NR-4ATP in 20 % ethanol solution (*red*), and aggregated Au NR after heating in 20 % ethanol (*blue*). (B) Photograph of Au NR-4ATP reacted with various concentrations of nitrite after incubation in 20 % ethanol at 95 °C. Reprinted with permission from Ref. [73], Copyright 2009, American Chemical Society. **c** Schematic illustration for the colorimetric sensing of NO_2^- based on etching of Au NR; Absorption spectra of GNRs after incubation with different concentrations of NO_2^- for 20 min. *Insets* show the decrease of absorption area response to different concentrations of NO_2^- and the color change with the increase of NO_2^- concentration from *left* to *right*, respectively. Reprinted with permission from Ref. [74], Copyright 2012, Royal Society of Chemistry

interaction between TNT and cysteamine at the surface of Au NP led to the aggregation of Au NPs and the color changed to violet blue, that can be readily seen by the naked eye. The strong D–A interaction between TNT and cysteamine and the good analytical properties of Au NPs described in previous reports substantially enable a picomolar amount of TNT (0.5 pM $\sim$ 5 nM) to be visualized by the naked eye (Fig. 2.18B). This study essentially offers a new and simple but sensitive method for TNT detection.

Dopamine (DA) plays a central role in brain functions such as reward-related behavior, movement, and mood. Shi's group first reported a direct, selective and

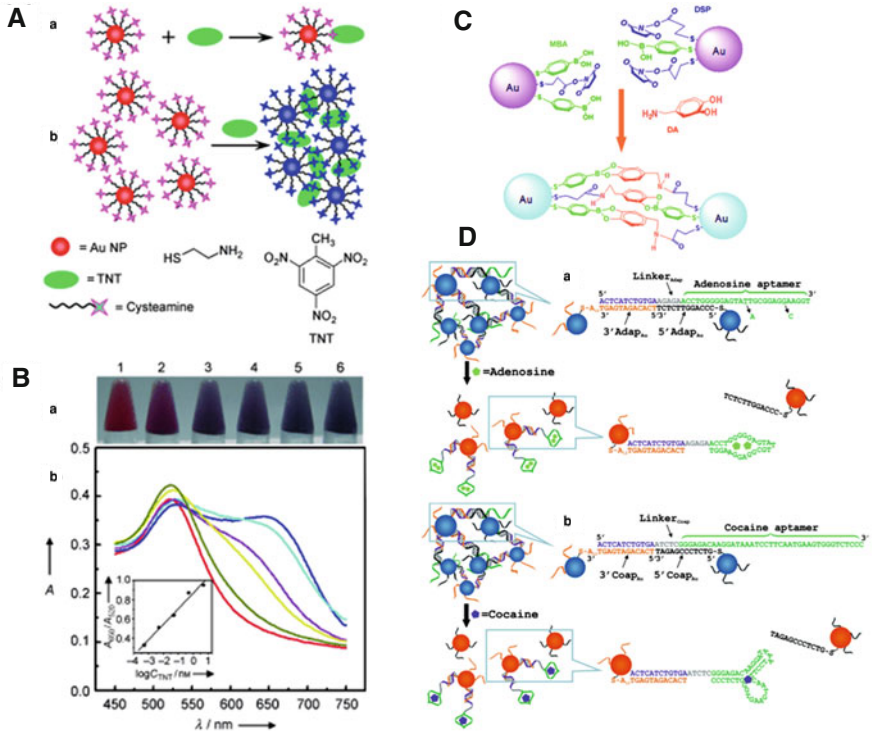

Fig. 2.18 **A D–A** interaction between cysteamine and TNT. (b) Assay for direct colorimetric visualization of TNT based on the electron **D–A** interaction at the Au NP/solution interface. **B** Colorimetric visualization of TNT by using Au NPs (containing 500 nm cysteamine). TNT concentrations varied from 5×10^{-13} M (2) to 5×10^{-9} M (6). (b) UV/Vis spectra of the Au NPs suspension (10 nm) containing 500 nm cysteamine in the presence of different concentrations of TNT: *red*, 0 m; *dark yellow*, 5×10^{-13} M; *yellow*, 5×10^{-12} M; *magenta*, 5×10^{-11} M; *cyan*, 5×10^{-10} M; *blue*, 5×10^{-9} M. *Inset* plot of A_{650}/A_{520} against log C_{TNT} for TNT assay. Reprinted with permission from Ref. [78]. Copyright 2008, Wiley. **C** Colorimetric detection of dopamine using functionalized gold nanoparticles (the MBA-DSP-AuNPs probe). Reprinted with permission from Ref. [81]. Copyright 2011, Wiley. **D** (a) Schematic representation of colorimetric detection of adenosine. The DNA sequences are shown in the *right side* of the figure. The A12 in 3'Adap Au denotes a 12-mer polyadenine chain. In a control experiment, a mutated linker with the two mutations shown by the two short *black arrows* was used. Note: The drawing is not to scale. (b) Schematic representation of the colorimetric detection of cocaine based on cocaine-induced disassembly of nanoparticle aggregates linked by a cocaine aptamer. Reprinted with permission from Ref. [87]. Copyright 2005, Wiley

sensitive strategy for the colorimetric visualization of cerebral DA at nanomolar levels using 4-mercaptophenylboronic acid (MBA) and dithiobis(succinimidyl-propionate) (DSP) cofunctionalized Au NPs [81]. MBA and DSP not only act as stabilizers for Au NPs but also interact with diols and amine functional groups, respectively, in DA to doubly recognize DA with high specificity (Fig. 2.18C). Double interactions between the functionalized Au NPs and DA triggered Au NP

aggregation, thus resulting in a color change from wine red to blue and to direct colorimetric visualization of DA.

Lu reported a general method to construct sensors based on a color change of Au NPs for any aptamer of interest [87]. The sensor was made of nanoparticle aggregates containing three components: two kinds of ssDNA-modified Au NPs and a linker DNA molecule that carries adenosine aptamer (Fig. 2.18D–a). Initially, Au NPs and the linker DNA were suspended in solution to generate purple Au NPs. In the Au NP aggregation process, the linker DNA molecule pairs respectively with two ssDNA-functionalized Au NPs where a part of adenosine aptamer also takes part in the DNA hybridization process. With the presence of adenosine, the aptamer changes its structure to bind with adenosine, resulting in the disassembly of the AuNP aggregates with a concomitant blue-to-red color change. Utilizing this system, adenosine was detected in concentrations from 0.3 to 2 mM. Similarly, a colorimetric sensor for cocaine was further constructed using a cocaine aptamer (Fig. 2.18D–b).

Chiral recognition is among the important and special modes of molecular recognition. Ye et al. developed an enantioseparation and detection platform for D- and L-cysteine using uridine 5'-triphosphate (UTP)-capped silver nanoparticles [96]. As seen in Fig. 2.19-1, in the presence of D-Cys, an appreciable yellow-to-red color shift of UTP-capped AgNPs can be observed, while no color changes were found in the presence of L-Cys. The limit of discrimination concentration between L- and D-Cys is approximately 100 nM (Fig. 2.19-2). UTP-capped AgNPs selectively interacted with one enantiomer of cysteine from a solution of racemic cysteine, leaving an excess of the other enantiomer in the solution after centrifugation treatment, thus resulting in enantioselective separation (Fig. 2.19-3).

2.3.3 Detection of Oligonucleotides

Nucleic acid-based detection has attracted great interest for early diagnosis of many diseases including cancer. Nanoparticle-based colorimetric assays have been demonstrated to be a highly competitive technology for oligonucleotides targets on the basis of highly specific base-paring of DNA strands [33]. Au NPs aggregate with concomitant color change is trigged by the presence of target oligonucleotides as a result of hybridization of the DNA strand. Fabrication of Au NPs functionalized with thiolated DNA strand allowed researchers to tailor the properties of the nanoparticle probes according to the assay method. This discovery has stimulated extensive use of oligonucleotide-directed Au NP aggregation for colorimetric detection of oligonucleotides. Recently, Gao and coworkers reported a method to conduct the detection of DNA target under extremely low salt conditions where the secondary structures are less stable and more accessible [98]. In this approach, a new type of nanoparticle probes prepared by functionalizing gold nanoparticles with nonionic morpholino oligos is employed. Because of the salt-

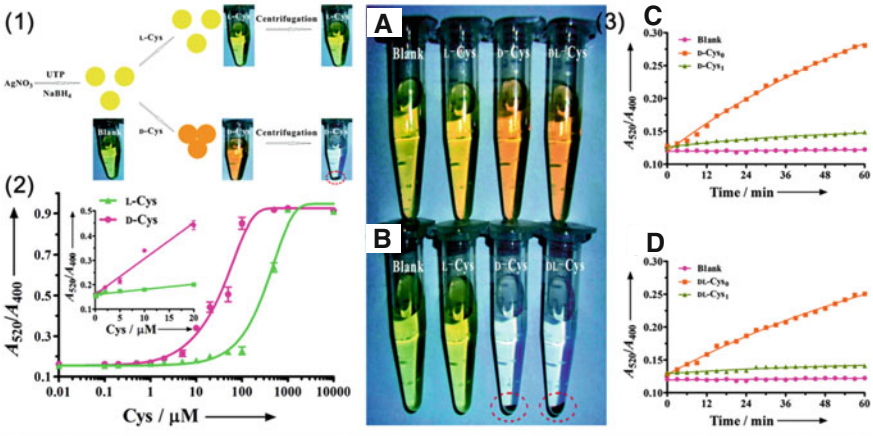

Fig. 2.19 **1** Colorimetric discrimination of L-and D-Cys using UTP-capped AgNPs. **2** Plots of A_{520}/A_{400} ratio of UTP-capped AgNPs upon the addition of l- and d-Cys at different concentrations (0.01, 0.1, 0.2, 0.5, 1, 2, 5, 10, 20, 50, 100, 500, 1,000, and 10,000 μM). *Inset* magnification of the plots in the range of 0.0–20 μM. The reaction time was 60 min, and then, the A_{520}/A_{400} ratios were collected. **3** Photo exhibition of UTP-capped AgNPs toward 100 μM l-Cys, d-Cys, and dl-Cys (A) before centrifugation and (B) after centrifugation. Plots of absorption ratios (A_{520}/A_{400}) corresponding to (C) 10 μM d-Cys0 and d-Cys1 (the supernatant of 100 μM d-Cys0 reacted with UTP-capped AgNPs) and (D) 10 μM dl-Cys0 and dl-Cys1 (the supernatant of 100 μM dl-Cys0 reacted with UTP-capped AgNPs). Reproduced with permission from Ref. [96]. Copyright 2011, American Chemical Society

independent hybridization of the probes with nucleic acid targets, nanoparticle assemblies can be formed in 2 mM Tris buffer solutions containing 0–5 mM NaCl, leading to the colorimetric target recognition (Fig. 2.20A). In this study, sharp melting transitions were observed in this method when a small amount of NaCl was presented. The melting behavior enables the unambiguous discrimination of the sequences with single-base substitution, deletion, or insertion [98]. Su and coworkers developed a label-free homogeneous phase bioassay to characterize the DNA binding properties of single-stranded DNA binding (SSB) protein using unmodified Au NPs and its application for detection of single nucleotide polymorphisms [97]. As shown in Fig. 2.20B, mismatched ssDNA can bind to SSB and form a SSB-ssDNA complex, which can protect Au NPs from salt-induced aggregation, while the complementary DNA can not, the Au NPs aggregated in the presence of salt (KCl). In this study, the detection of DNA hybridization with single nucleotide polymorphism selectivity was further developed. Owing to the high affinity between SSB and dissociated ssDNA, single-base mismatch discrimination in a long sequence of 30-mer DNA was achieved for both the end- and center-base mismatch.

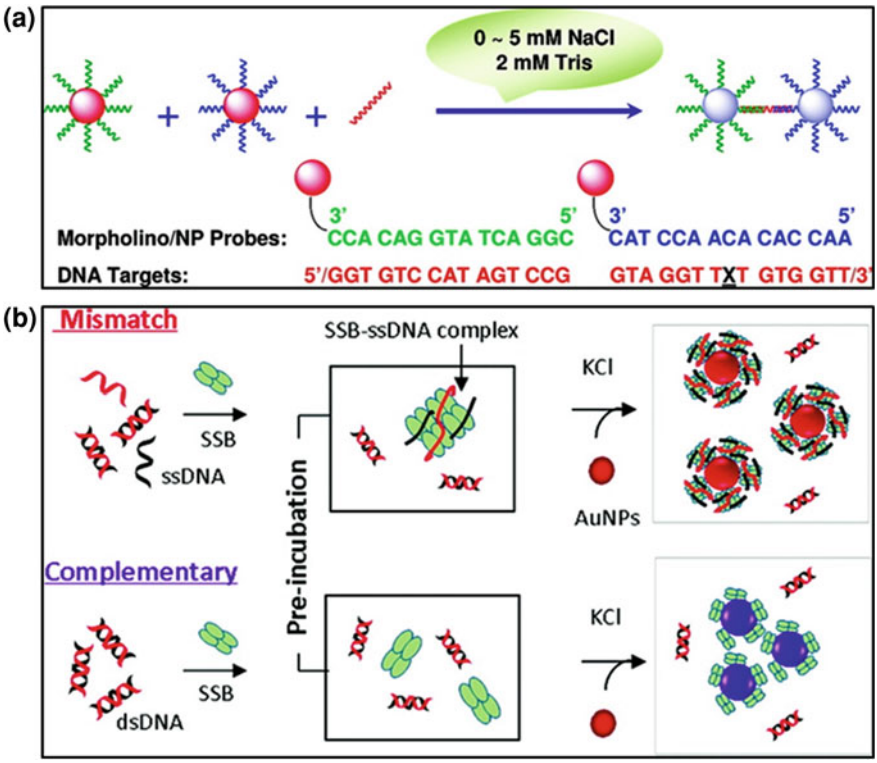

Fig. 2.20 **A** Schematic presentation of the colorimetric detection of nucleic acids under extremely low salt conditions. Reprinted with permission from Ref. [98]. Copyright 2011, American Chemical Society. **B** Schematic illustrations of DNA detection principle based on the inverse relationship between sequence-dependent DNA hybridization efficiency and the tendency of forming large SSB–ssDNA complex to protect AuNPs from salt-induced aggregation. Reprinted with permission from Ref. [97]. Copyright 2011, American Chemical Society

2.3.4 Detection of Proteins

Colorimetric nanoprobes have been extensively developed for the detection of disease associated biomarker proteins or irregular proteins, such as platelet-derived growth factors (PDGFs) and their receptors, thrombin, histone-modifying enzymes, as summarized in Table 2.1.

Chang and coworkers developed a highly specific sensing system for PDGFs and platelet-derived growth factor receptors (PDGFR) using aptamer-modified Au NPs [101]. Au NPs modified with an aptamer (Apt-AuNPs) that is specific to PDGFs was used in this study. The Apt-Au NP solutions change color in the presence of PDGF at high enough concentration, where PDGF molecules act as bridges that link Apt-AuNPs together. At very high PDGF concentrations, there was no obvious aggregation owing to the repulsion and steric effects because the

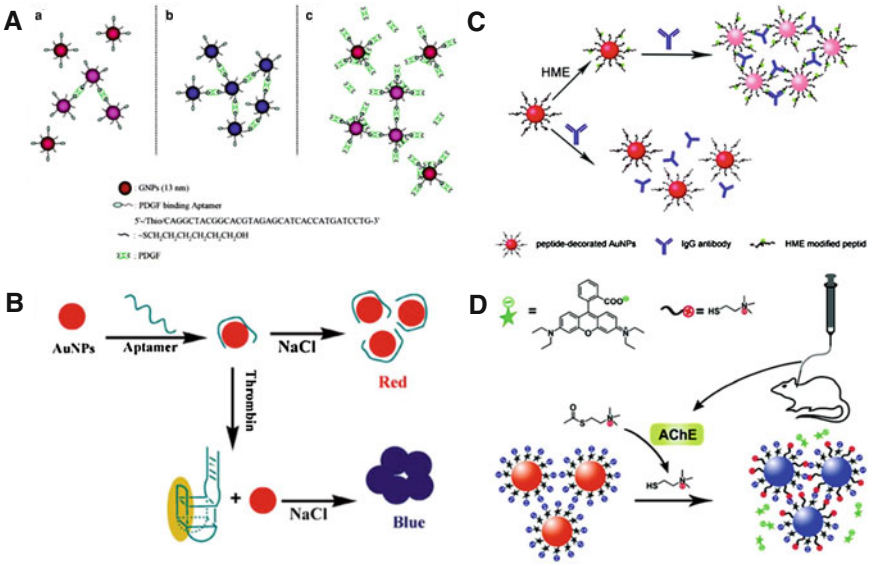

Fig. 2.21 **a** Schematic representation of the aggregation of Apt-Au NPs in the presence of PDGFs at Low, (B) Medium, and (C) High Concentrations. Reproduced with permission from Ref. [101]. Copyright 2005, American Chemical Society. **b** AuNPs colorimetric strategy for thrombin detection. Reproduced with permission from Ref. [99]. Copyright 2007, Royal Society of Chemistry. **c** Illustration of biosensing strategy for Histone-Modifying Enzyme (HME) based on antibody-mediated assembly of Au NPs decorated with substrate peptides subjected to enzymatic modifications. Reproduced with permission from Ref. [100]. Copyright 2012, American Chemical Society. **d** The detection (colorimetric and fluorometric) of AChE based on RB-Au NPs. The well-dispersed RB-Au NPs (*red*) are induced to aggregate (*purple*) via electrostatic interaction in the presence of thiocholine derived from the hydrolysis of ATC catalyzed by AChE in the CSF of transgenic mice, accompanied with the fluorescence recovery of RB (the color of the stars changed from *gray* to *green*). Reproduced with permission from Ref. [103]. Copyright 2012, Wiley

surface of the Au NPs became saturated with PDGF molecules through aptamer-PDGF binding, as shown in Fig. 2.21a. Utilizing this system, the detection limit of PDGFs was as low as 2.5 and 3.2 nM for PDGF receptor.

Dong's group reported aptamer-based colorimetric sensing of alpha-thrombin using unmodified Au NPs [99]. Thrombin binding aptamer (TBA) is much more inclined to fold into a structure of G-quadruplex/duplex when interacts with thrombin. In the absence of thrombin, unfold TBA could protect Au NPs from salt-induced aggregation and the solution remained red color. With the addition of thrombin, TBA interacted with thrombin and folded into a structure of G-quadruplex/duplex, resulting in the aggregation of AuNPs after the addition of NaCl as shown in Fig. 2.21b. The color of AuNPs colloidal solution changed from red to purple. The change of TBA conformation from the unfolded one to G-quadruplex/duplex could be directly observed with the naked eye, realizing the detection of protein thrombin in a very convenient way from 0 to 167 nM with a detection limit of 0.83 nM.

Enzymatic immuno-assembly of Au NPs for visualized activity screening of histone-modifying enzymes (HME) has been developed by Liu and coworkers [100]. This strategy relies on the antibody-mediated assembly of AuNPs decorated with substrate peptides that are subjected to enzymatic modifications by the HME Fig. 2.21c. The Au NP was decorated with a substrate peptide containing a substrate sequence at the N' terminal and a thiolated, negatively charged spacer sequence at the C' terminal. In the presence of an active HME such as HMT or HAT, the substrate peptide is modified at a specified site with a certain group such as methyl for HMT or acetyl for HAT. After the addition of an immunoglobin G (IgG) antibody specific to this modified peptide (a methylated peptide sequence for HMT or an acetylated peptide sequence for HAT), the peptides subjected to enzymatic modifications can be bound by the divalent IgG antibody at its two binding sites. This triggers a network-like assembly of the peptide-modified AuNP and thus induces a significant variation in the plasmon resonance absorption peak with a visualized color change. A quasilinear correlation was obtained to the logarithmic concentration of HMT ranging from 1 to 200 nM with a detection limit of 0.2, 50 nM to 20 μM for inhibitors of HMT, 2–200 nM with the detection limit estimated to be 0.5 nM for HAT.

Jiang's group provided a highly sensitive and selective rhodamine B-modified gold nanoparticle (RB-Au NP)-based assay with dual readouts (colorimetric and fluorometric) for monitoring the levels of acetylcholinesterase (AChE) in the cerebrospinal fluid (CSF) of transgenic mice suffering from Alzheimer's disease (AD) [103]. In this study, upon the addition of both acetylthilcholine (ATC, an analog of acetylcholine) and AChE into a RB-Au NPs solution, AChE could hydrolyze ATC to generate thiocholine, which strongly binded onto surfaces of Au NPs via the formation of Au–S bond to replace RB molecules, resulting in the desorption of RB molecules from Au surfaces. Thiocholine and the residual RB molecules attached to different Au NP surfaces may be able to interact via electrostatic interaction between the quaternary ammonium group on thiocholine and the acidic group on RB and cause the aggregation of Au NPs, as shown in Fig. 2.21d. This process resulted in a rapid change of the absorption band as well as the color change of the AuNPs solution from red to blue. In addition, when AChE inhibitors were present, AChE failed to catalyze ATC to generate the thiocholine thus the RB-AuNPs remained dispersed. For the colorimetric response, the detection limit can reach 1.0 mU/mL.

2.3.5 Sensing of Cancer Cells

The key to the effective and ultimately successful treatment of diseases such as cancer is early and accurate diagnosis. Colorimetric sensing of cancer cell does act as an attractive method based on the aptamer and specific antibody-conjugated nanoparticles. The aptamers are selected using the cell-SELEX methodology in which live whole cells served as the target. Tan and coworkers have developed a

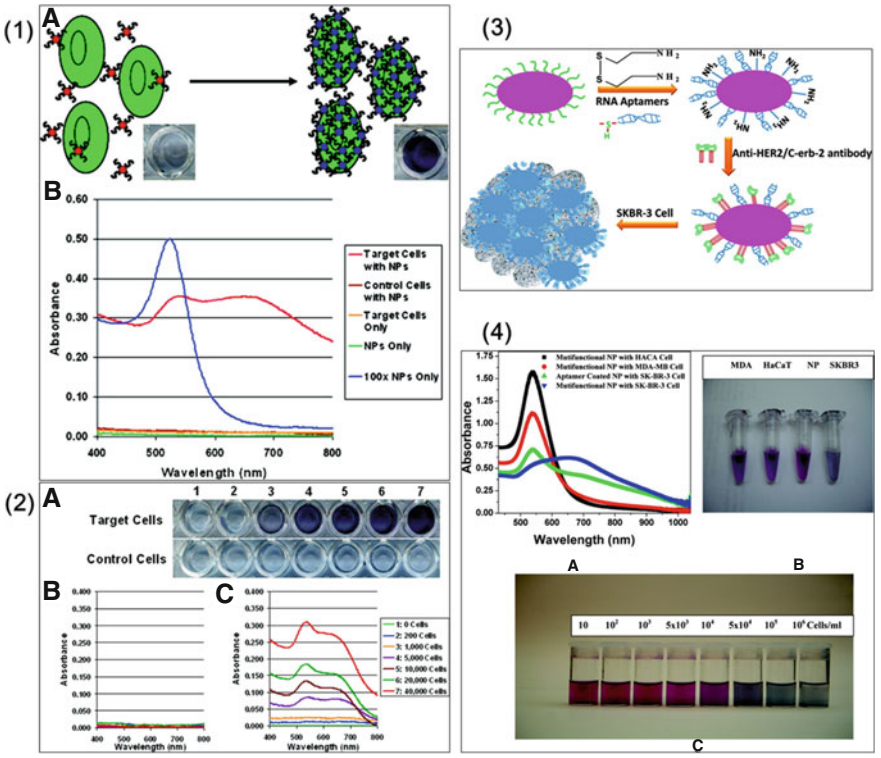

Fig. 2.22 **1** (A) Schematic representation of the aptamer-conjugated Au NP based colorimetric assay. (B) Plots depicting the absorption spectra obtained for various samples analyzed using aptamer-conjugated Au NPs. The spectra illustrate the differences in spectral characteristics observed after the aptamer-conjugated Au NPs bind to the target cells. **2** Images of aptamer-conjugated Au NPs with increasing amounts of target (*top*) and control cells (*bottom*). The amount of cells used in each sample is given in the legend on the bottom right. (B) Absorption spectra of the control cell samples with aptamer-conjugated Au NPs. (C) Absorption spectra of the target samples with aptamer-conjugated Au NPs. Reproduced with permission from Ref. [105]. Copyright 2008, American Chemical Society. **3** First two steps show schematic representation of the synthesis of monoclonal anti-HER2 antibody and S6 RNA aptamer-conjugated *oval-shaped* gold nanoparticles. Third step shows schematic representation of multifunctional *oval-shaped* gold-nanoparticle-based sensing of the SK-BR-3 breast cancer cell line. **4** (A) Absorption profile variation of multifunctional *oval-shaped* gold nanoparticles due to the addition of different cancerous and noncancerous cells. (B) Photograph showing colorimetric change upon addition of different cancer cells (10^4 cells/mL). (C) Photograph demonstrating colorimetric change upon the addition of different numbers of SK-BR-3 cells. Reproduced with permission from Ref. [106]. Copyright 2010, American Chemical Society

colorimetric assay for the direct detection of diseased cells [105]. In this study, the aptamer-conjugated Au NPs (20 nm) were targeted to assemble on the surface of a specific type of cancer cell through the recognition of the aptamer to its target on the cell membrane surface, inducing a distinct color change as shown in Fig. 2.22-

1A. The assembly of Au NPs around the target cells caused an increase in the absorption and scattering of the solution Fig. 2.22-1B. This colorimetric assay can realize the quantitative analysis of target cells (Fig. 2.22-2) and showed excellent sensitivity with both the naked eye and based on absorbance measurements with a detection limit calculated to be 90 cells.

In addition to the aptamer-conjugated nanoparticles, antibody-functionalized nanoparticles also can act as effective recognition moiety for the colorimetric selective sensing of cancer cells. Ray group reported simple colorimetric assay for breast cancer SK-BR-3 cell lines using a multifunctional (monoclonal anti-HER2/c-erb-2 antibody and S6 RNA aptamer-conjugated) oval-shaped Au NP-based nanoconjugate [106]. As shown in Fig. 2.22-3, the functionalized nanoparticles were initially fabricated through two steps; then in the presence of the breast cancer SK-BR-3 cell line, several nanoparticles can bind to HER2 receptors in the cancer cell, producing nanoparticle aggregates. Colorimetric change was observed after the addition of cancer cells as seen from Fig. 2.22-4. The use of antibody and aptamer cofunctionalized nanoconjugate platform fabricated a highly selective and sensitive detection method for a breast cancer cell line at a 100 cells/mL level.

References

1. Kelly KL, Coronado E, Zhao LL, Schatz GC (2003) The optical properties of metal nanoparticles: the influence of size, shape, and dielectric environment. J Phys Chem B 107:668–677
2. Ray PC (2010) Size and shape dependent second order nonlinear optical properties of nanomaterials and their application in biological and chemical sensing. Chem Rev 110:5332–5365
3. Halas NJ, Lal S, Chang WS, Link S, Nordlander P (2011) Plasmons in strongly coupled metallic nanostructures. Chem Rev 111:3913–3961
4. Jain PK, Huang X, El-Sayed IH, El-Sayed MA (2008) Noble metals on the nanoscale: optical and photothermal properties and some applications in imaging, sensing, biology, and medicine. Acc Chem Res 41:1578–1586
5. Wang Z, Ma L (2009) Gold nanoparticle probes. Coord Chem Rev 253:1607–1618
6. Boisselier E, Astruc D (2009) Gold nanoparticles in nanomedicine: preparations, imaging, diagnostics, therapies and toxicity. Chem Soc Rev 38:1759–1782
7. Saha K, Agasti SS, Kim C, Li X, Rotello VM (2012) Gold nanoparticles in chemical and biological sensing. Chem Rev 112:2739–2779
8. Wilson R (2008) The use of gold nanoparticles in diagnostics and detection. Chem Soc Rev 37:2028–2045
9. Motl NE, Smith AF, DeSantisa CJ, Skrabalak SE (2014) Engineering plasmonic metal colloids through composition and structural design. Chem Soc Rev. doi:10.1039/C3CS60347D
10. Zhang JZ, Noguez C (2008) Plasmonic optical properties and applications of metal nanostructures. Plasmonics 3:127–150
11. Haes AJ, Haynes CL, McFarland AD, Schatz GC, Van Duyne RP, Zou S (2005) Plasmonic materials for surface-enhanced sensing and spectroscopy. MRS Bull 30:368–375

12. Jain PK, Lee KS, El-Sayed IH, El-Sayed MA (2006) Calculated absorption and scattering properties of gold nanoparticles of different size, shape, and composition: applications in biological imaging and biomedicine. J Phys Chem B 110:7238–7248
13. Link S, El-Sayed MA (2003) Optical properties and ultrafast dynamics of metallic nanocrystals. Annu Rev Phys Chem 54:331–366
14. Griffin J, Singh AK, Senapati D, Lee E, Gaylor K, Jones-Boone J, Ray PC (2009) Sequence-specific HCV RNA quantification using the size-dependent nonlinear optical properties of gold nanoparticles. Small 5:839–845
15. Link S, El-Sayed MA (1999) Spectral properties and relaxation dynamics of surface plasmon electronic oscillations in gold and silver nanodots and nanorods. J Phys Chem B 103:8410–8426
16. Ye X, Jin L, Caglayan H, Chen J, Xing G, Zheng C, Doan-Nguyen V, Kang Y, Engheta N, Kagan CR (2012) Improved size-tunable synthesis of monodisperse gold nanorods through the use of aromatic additives. ACS Nano 6:2804–2817
17. Jakab A, Rosman C, Khalavka Y, Becker J, Trügler A, Hohenester U, Sönnichsen C (2011) Highly sensitive plasmonic silver nanorods. ACS Nano 5:6880–6885
18. Jones MR, Osberg KD, Macfarlane RJ, Langille MR, Mirkin CA (2011) Templated techniques for the synthesis and assembly of plasmonic nanostructures. Chem Rev 111:3736–3827
19. Murphy CJ, Thompson LB, Alkilany AM, Sisco PN, Boulos SP, Sivapalan ST, Yang JA, Chernak DJ, Huang J (2010) The many faces of gold nanorods. J Phys Chem Lett 1:2867–2875
20. Zeng J, Roberts S, Xia Y (2010) Nanocrystal-based time–temperature indicators. Chem Eur J 16:12559–12563
21. Singh AK, Senapati D, Neely A, Kolawole G, Hawker C, Ray PC (2009) Nonlinear optical properties of triangular silver nanomaterials. Chem Phys Lett 481:94–98
22. Becker J, Zins I, Jakab A, Khalavka Y, Schubert O, Sönnichsen C (2008) Plasmonic focusing reduces ensemble linewidth of silver-coated gold nanorods. Nano Lett 8:1719–1723
23. Xiang Y, Wu X, Liu D, Li Z, Chu W, Feng L, Zhang K, Zhou W, Xie S (2008) Gold nanorod-seeded growth of silver nanostructures: from homogeneous coating to anisotropic coating. Langmuir 24:3465–3470
24. Park G, Lee C, Seo D, Song H (2012) Full-color tuning of surface plasmon resonance by compositional variation of Au@Ag core-shell nanocubes with sulfides. Langmuir 28:9003–9009
25. Su K-H, Wei Q-H, Zhang X, Mock J, Smith DR, Schultz S (2003) Interparticle coupling effects on plasmon resonances of nanogold particles. Nano Lett 3:1087–1090
26. Daniel M-C, Astruc D (2004) Gold nanoparticles: assembly, supramolecular chemistry, quantum-size-related properties, and applications toward biology, catalysis, and nanotechnology. Chem Rev 104:293–346
27. Liu M, Guyot-Sionnest P (2004) Synthesis and optical characterization of Au/Ag core/shell nanorods. J Phys Chem B 108:5882–5888
28. Ma Y, Li W, Cho EC, Li Z, Yu T, Zeng J, Xie Z, Xia Y (2010) Au@ Ag core–shell nanocubes with finely tuned and well-controlled sizes, shell thicknesses, and optical properties. ACS Nano 4:6725–6734
29. Srivastava S, Frankamp BL, Rotello VM (2005) Controlled plasmon resonance of gold nanoparticles self-assembled with PAMAM dendrimers. Chem Mater 17:487–490
30. Chen L, Lou TT, Yu CW, Kang Q, Chen LX (2011) N-1-(2-mercaptoethyl)thymine modification of gold nanoparticles: a highly selective and sensitive colorimetric chemosensor for Hg^{2+}. Analyst 136:4770–4773
31. Zhou Y, Wang S, Zhang K, Jiang X (2008) Visual detection of copper(II) by azide- and alkyne-functionalized gold nanoparticles using click chemistry. Angew Chem Int Ed 47:7454–7456

32. Cao R, Li B, Zhang Y, Zhang Z (2011) Naked-eye sensitive detection of nuclease activity using positively-charged gold nanoparticles as colorimetric probes. Chem Commun 47:12301–12303
33. Elghanian R, Storhoff JJ, Mucic RC, Letsinger RL, Mirkin CA (1997) Selective colorimetric detection of polynucleotides based on the distance-dependent optical properties of gold nanoparticles. Science 277:1078–1081
34. Ai K, Liu Y, Lu L (2009) Hydrogen-bonding recognition-induced color change of gold nanoparticles for visual detection of melamine in raw milk and infant formula. J Am Chem Soc 131:9496–9497
35. Rosi NL, Mirkin CA (2005) Nanostructures in biodiagnostics. Chem Rev 105:1547–1562
36. Li D, Wieckowska A, Willner I (2008) Optical analysis of Hg^{2+} ions by oligonucleotide–gold-nanoparticle hybrids and DNA-based machines. Angew Chem Int Ed 120:3991–3995
37. Fu XL, Chen LX, Li JH, Lin M, You HY, Wang WH (2012) Label-free colorimetric sensor for ultrasensitive detection of heparin based on color quenching of gold nanorods by graphene oxide. Biosens Bioelectron 34:227–231
38. Lou TT, Chen ZP, Wang YQ, Chen LX (2011) Blue-to-red colorimetric sensing strategy for Hg(2+) and Ag(+) via redox-regulated surface chemistry of gold nanoparticles. ACS Appl Mater Interfaces 3:1568–1573
39. Chen Y-Y, Chang H-T, Shiang Y-C, Hung Y-L, Chiang C-K, Huang C-C (2009) Colorimetric assay for lead ions based on the leaching of gold nanoparticles. Anal Chem 81:9433–9439
40. Malile B, Chen JI (2013) Morphology-based plasmonic nanoparticle sensors: controlling etching kinetics with target-responsive permeability gate. J Am Chem Soc 135:16042–16045
41. Rex M, Hernandez FE, Campiglia AD (2006) Pushing the limits of mercury sensors with gold nanorods. Anal Chem 78:445–451
42. Lou TT, Chen LX, Chen ZP, Wang YQ, Chen L, Li JH (2011) Colorimetric detection of trace copper ions based on catalytic leaching of silver-coated gold nanoparticles. ACS Appl Mater Interfaces 3:4215–4220
43. Wang XK, Chen L, Chen LX (2013) Colorimetric determination of copper ions based on the catalytic leaching of silver from the shell of silver-coated gold nanorods. Microchim Acta 181:105–110
44. Wang GQ, Chen ZP, Chen LX (2011) Mesoporous silica-coated gold nanorods: towards sensitive colorimetric sensing of ascorbic acid via target-induced silver overcoating. Nanoscale 3:1756–1759
45. Xia Y, Ye J, Tan K, Wang J, Yang G (2013) Colorimetric visualization of glucose at the submicromole level in serum by a homogenous silver nanoprism-glucose oxidase system. Anal Chem 85:6241–6247
46. Lee JS, Han MS, Mirkin CA (2007) Colorimetric detection of mercuric ion (Hg^{2+}) in aqueous media using DNA-functionalized gold nanoparticles. Angew Chem Int Ed 46:4093–4096
47. Huang CC, Chang HT (2007) Parameters for selective colorimetric sensing of mercury(II) in aqueous solutions using mercaptopropionic acid-modified gold nanoparticles. Chem Commun 12:1215–1217
48. Xue X, Wang F, Liu X (2008) One-step, room temperature, colorimetric detection of mercury (Hg^{2+}) using DNA/nanoparticle conjugates. J Am Chem Soc 130:3244–3245
49. Yu CJ, Cheng TL, Tseng WL (2009) Effects of Mn^{2+} on oligonucleotide-gold nanoparticle hybrids for colorimetric sensing of Hg^{2+}: improving colorimetric sensitivity and accelerating color change. Biosens Bioelectron 25:204–210
50. Xu Y, Deng L, Wang H, Ouyang X, Zheng J, Li J, Yang R (2011) Metal-induced aggregation of mononucleotides-stabilized gold nanoparticles: an efficient approach for simple and rapid colorimetric detection of Hg(II). Chem Commun 47:6039–6041

51. Lou T, Chen L, Zhang C, Kang Q, You H, Shen D, Chen L (2012) A simple and sensitive colorimetric method for detection of mercury ions based on anti-aggregation of gold nanoparticles. Anal Methods 4:488
52. Wang GL, Zhu XY, Jiao HJ, Dong YM, Li ZJ (2012) Ultrasensitive and dual functional colorimetric sensors for mercury (II) ions and hydrogen peroxide based on catalytic reduction property of silver nanoparticles. Biosens Bioelectron 31:337–342
53. Chen L, Fu XL, Lu WH, Chen LX (2013) Highly sensitive and selective colorimetric sensing of Hg^{2+} based on the morphology transition of silver nanoprisms. ACS Appl Mater Interfaces 5:284–290
54. Lin C-Y, Yu C-J, Lin Y-H, Tseng W-L (2010) Colorimetric sensing of silver (I) and mercury (II) ions based on an assembly of Tween 20-stabilized gold nanoparticles. Anal Chem 82:6830–6837
55. Guo Y, Wang Z, Qu W, Shao H, Jiang X (2011) Colorimetric detection of mercury, lead and copper ions simultaneously using protein-functionalized gold nanoparticles. Biosens Bioelectron 26:4064–4069
56. Wang Z, Lee JH, Lu Y (2008) Label-free colorimetric detection of lead ions with a nanomolar detection limit and tunable dynamic range by using gold nanoparticles and DNAzyme. Adv Mater 20:3263–3267
57. Chai F, Wang C, Wang T, Li L, Su Z (2010) Colorimetric detection of Pb^{2+} using glutathione functionalized gold nanoparticles. ACS Appl Mater Interfaces 2:1466–1470
58. Kalluri JR, Arbneshi T, Khan SA, Neely A, Candice P, Varisli B, Washington M, McAfee S, Robinson B, Banerjee S, Singh AK, Senapati D, Ray PC (2009) Use of gold nanoparticles in a simple colorimetric and ultrasensitive dynamic light scattering assay: selective detection of arsenic in groundwater. Angew Chem Int Ed 48:9668–9671
59. Xue Y, Zhao H, Wu Z, Li X, He Y, Yuan Z (2011) Colorimetric detection of Cd^{2+} using gold nanoparticles cofunctionalized with 6-mercaptonicotinic acid and L-cysteine. Analyst 136:3725–3730
60. Dang YQ, Li HW, Wang B, Li L, Wu Y (2009) Selective detection of trace Cr^{3+} in aqueous solution by using 5,5'-dithiobis (2-nitrobenzoic acid)-modified gold nanoparticles. ACS Appl Mater Interfaces 1:1533–1538
61. Li F-M, Liu J-M, Wang X-X, Lin L-P, Cai W-L, Lin X, Zeng Y-N, Li Z-M, Lin S-Q (2011) Non-aggregation based label free colorimetric sensor for the detection of Cr (VI) based on selective etching of gold nanorods. Sensor Actuators B Chem 155:817–822
62. Zhang Z, Zhang J, Lou T, Pan D, Chen L, Qu C, Chen Z (2012) Label-free colorimetric sensing of cobalt(II) based on inducing aggregation of thiosulfate stabilized gold nanoparticles in the presence of ethylenediamine. Analyst 137:400–405
63. Ma YR, Niu HY, Zhang XL, Cai YQ (2011) Colorimetric detection of copper ions in tap water during the synthesis of silver/dopamine nanoparticles. Chem Commun 47:12643–12645
64. Wang SS, Chen ZP, Chen L, Liu RL, Chen LX (2013) Label-free colorimetric sensing of copper(II) ions based on accelerating decomposition of H2O2 using gold nanorods as an indicator. Analyst 138:2080–2084
65. Chen ZP, Liu RL, Wang SS, Qu CL, Chen LX, Wang Z (2013) Colorimetric sensing of copper(ii) based on catalytic etching of gold nanorods. RSC Adv 3:13318
66. Hung YL, Hsiung TM, Chen YY, Huang CC (2010) A label-free colorimetric detection of lead ions by controlling the ligand shells of gold nanoparticles. Talanta 82:516–522
67. Lin S-Y, Liu S-W, Lin C-M, Chen C-H (2002) Recognition of potassium ion in water by 15-crown-5 functionalized gold nanoparticles. Anal Chem 74:330–335
68. Lin S-Y, Chen C-H, Lin M-C, Hsu H-F (2005) A cooperative effect of bifunctionalized nanoparticles on recognition: sensing alkali ions by crown and carboxylate moieties in aqueous media. Anal Chem 77:4821–4828
69. Kim S, Kim J, Lee NH, Jang HH, Han MS (2011) A colorimetric selective sensing probe for calcium ions with tunable dynamic ranges using cytidine triphosphate stabilized gold nanoparticles. Chem Commun 47:10299–10301

70. Eom MS, Jang W, Lee YS, Choi G, Kwon YU, Han MS (2012) A bi-ligand co-functionalized gold nanoparticles-based calcium ion probe and its application to the detection of calcium ions in serum. Chem Commun 48:5566–5568
71. Lisowski CE, Hutchison JE (2009) Malonamide-functionalized gold nanoparticles for selective, colorimetric sensing of trivalent lanthanide ions. Anal Chem 81:10246–10253
72. Daniel WL, Han MS, Lee J-S, Mirkin CA (2009) Colorimetric nitrite and nitrate detection with gold nanoparticle probes and kinetic end points. J Am Chem Soc 131:6362–6363
73. Xiao N, Yu C (2010) Rapid-response and highly sensitive noncross-linking colorimetric nitrite sensor using 4-aminothiophenol modified gold nanorods. Anal Chem 82:3659–3663
74. Chen ZP, Zhang ZY, Qu CL, Pan DW, Chen LX (2012) Highly sensitive label-free colorimetric sensing of nitrite based on etching of gold nanorods. Analyst 137:5197–5200
75. Tripathy SK, Woo JY, Han CS (2011) Highly selective colorimetric detection of hydrochloric acid using unlabeled gold nanoparticles and an oxidizing agent. Anal Chem 83:9206–9212
76. Chen L, Lu WH, Wang XK, Chen LX (2013) A highly selective and sensitive colorimetric sensor for iodide detection based on anti-aggregation of gold nanoparticles. Sensor Actuators B Chem 182:482–488
77. Zhang ZY, Zhang J, Qu CL, Pan DW, Chen ZP, Chen LX (2012) Label free colorimetric sensing of thiocyanate based on inducing aggregation of Tween 20-stabilized gold nanoparticles. Analyst 137:2682–2686
78. Jiang Y, Zhao H, Zhu N, Lin Y, Yu P, Mao LQ (2008) A simple assay for direct colorimetric visualization of trinitrotoluene at picomolar levels using gold nanoparticles. Angew Chem Int Ed 47:8601–8604
79. Dasary SS, Senapati D, Singh AK, Anjaneyulu Y, Yu H, Ray PC (2010) Highly sensitive and selective dynamic light-scattering assay for TNT detection using p-ATP attached gold nanoparticle. ACS Appl Mater Interfaces 2:3455–3460
80. Radhakumary C, Sreenivasan K (2011) Naked eye detection of glucose in urine using glucose oxidase immobilized gold nanoparticles. Anal Chem 83:2829–2833
81. Kong B, Zhu A, Luo Y, Tian Y, Yu Y, Shi G (2011) Sensitive and selective colorimetric visualization of cerebral dopamine based on double molecular recognition. Angew Chem Int Ed 50:1837–1840
82. Feng JJ, Guo H, Li YF, Wang YH, Chen WY, Wang AJ (2013) Single molecular functionalized gold nanoparticles for hydrogen-bonding recognition and colorimetric detection of dopamine with high sensitivity and selectivity. ACS Appl Mater Interfaces 5:1226–1231
83. Guo L, Zhong J, Wu J, Fu F, Chen G, Zheng X, Lin S (2010) Visual detection of melamine in milk products by label-free gold nanoparticles. Talanta 82:1654–1658
84. Zhang Y, Li B, Xu C (2010) Visual detection of ascorbic acid via alkyne-azide click reaction using gold nanoparticles as a colorimetric probe. Analyst 135:1579–1584
85. Wang J, Wang L, Liu X, Liang Z, Song S, Li W, Li G, Fan C (2007) A gold nanoparticle-based aptamer target binding readout for ATP assay. Adv Mater 19:3943–3946
86. Liu J, Lu Y (2004) Adenosine-dependent assembly of aptazyme-functionalized gold nanoparticles and its application as a colorimetric biosensor. Anal Chem 76:1627–1632
87. Liu J, Lu Y (2005) Fast colorimetric sensing of adenosine and cocaine based on a general sensor design involving aptamers and nanoparticles. Angew Chem Int Ed 45:90–94
88. Zhang J, Wang L, Pan D, Song S, Boey FY, Zhang H, Fan C (2008) Visual cocaine detection with gold nanoparticles and rationally engineered aptamer structures. Small 4:1196–1200
89. Sun J, Ge J, Liu W, Fan Z, Zhang H, Wang P (2011) Highly sensitive and selective colorimetric visualization of streptomycin in raw milk using Au nanoparticles supramolecular assembly. Chem Commun 47:9888–9890
90. Zhang X, Zhao H, Xue Y, Wu Z, Zhang Y, He Y, Li X, Yuan Z (2012) Colorimetric sensing of clenbuterol using gold nanoparticles in the presence of melamine. Biosens Bioelectron 34:112–117

91. Kim YS, Kim JH, Kim IA, Lee SJ, Jurng J, Gu MB (2010) A novel colorimetric aptasensor using gold nanoparticle for a highly sensitive and specific detection of oxytetracycline. Biosens Bioelectron 26:1644–1649
92. Sun J, Guo L, Bao Y, Xie J (2011) A simple, label-free AuNPs-based colorimetric ultrasensitive detection of nerve agents and highly toxic organophosphate pesticide. Biosens Bioelectron 28:152–157
93. Zhang M, Liu YQ, Ye BC (2011) Rapid and sensitive colorimetric visualization of phthalates using UTP-modified gold nanoparticles cross-linked by copper(II). Chem Commun 47:11849–11851
94. Li L, Li B (2009) Sensitive and selective detection of cysteine using gold nanoparticles as colorimetric probes. Analyst 134:1361–1365
95. Sudeep P, Joseph SS, Thomas KG (2005) Selective detection of cysteine and glutathione using gold nanorods. J Am Chem Soc 127:6516–6517
96. Zhang M, Ye BC (2011) Colorimetric chiral recognition of enantiomers using the nucleotide-capped silver nanoparticles. Anal Chem 83:1504–1509
97. Tan YN, Lee KH, Su X (2011) Study of single-stranded DNA binding protein-nucleic acids interactions using unmodified gold nanoparticles and its application for detection of single nucleotide polymorphisms. Anal Chem 83:4251–4257
98. Zu Y, Ting AL, Yi G, Gao Z (2011) Sequence-selective recognition of nucleic acids under extremely low salt conditions using nanoparticle probes. Anal Chem 83:4090–4094
99. Wei H, Li B, Li J, Wang E, Dong S (2007) Simple and sensitive aptamer-based colorimetric sensing of protein using unmodified gold nanoparticle probes. Chem Commun 36:3735–3737
100. Zhen Z, Tang LJ, Long H, Jiang JH (2012) Enzymatic immuno-assembly of gold nanoparticles for visualized activity screening of histone-modifying enzymes. Anal Chem 84:3614–3620
101. Huang C-C, Huang Y-F, Cao Z, Tan W, Chang H-T (2005) Aptamer-modified gold nanoparticles for colorimetric determination of platelet-derived growth factors and their receptors. Anal Chem 77:5735–5741
102. Xue W, Zhang G, Zhang D (2011) A sensitive colorimetric label-free assay for trypsin and inhibitor screening with gold nanoparticles. Analyst 136:3136–3141
103. Liu D, Chen W, Tian Y, He S, Zheng W, Sun J, Wang Z, Jiang X (2012) A highly sensitive gold-nanoparticle-based assay for acetylcholinesterase in cerebrospinal fluid of transgenic mice with Alzheimer's disease. Adv Healthc Mater 1:90–95
104. Wu Z, Wu ZK, Tang H, Tang LJ, Jiang JH (2013) Activity-based DNA-gold nanoparticle probe as colorimetric biosensor for DNA methyltransferase/glycosylase assay. Anal Chem 85:4376–4383
105. Medley CD, Smith JE, Tang Z, Wu Y, Bamrungsap S, Tan W (2008) Gold nanoparticle-based colorimetric assay for the direct detection of cancerous cells. Anal Chem 80:1067–1072
106. Lu W, Arumugam SR, Senapati D, Singh AK, Arbneshi T, Khan SA, Yu H, Ray PC (2010) Multifunctional oval-shaped gold-nanoparticle-based selective detection of breast cancer cells using simple colorimetric and highly sensitive two-photon scattering assay. ACS Nano 4:1739–1749
107. Kim Y, Johnson RC, Hupp JT (2001) Gold nanoparticle-based sensing of "spectroscopically silen" heavy metal ions. Nano Lett 1:165–167
108. Beqa L, Singh AK, Khan SA, Senapati D, Arumugam SR, Ray PC (2011) Gold nanoparticle-based simple colorimetric and ultrasensitive dynamic light scattering assay for the selective detection of Pb(II) from paints, plastics, and water samples. ACS Appl Mater Interfaces 3:668–673
109. Wei H, Li B, Li J, Dong S, Wang E (2008) DNAzyme-based colorimetric sensing of lead (Pb(2+)) using unmodified gold nanoparticle probes. Nanotechnology 19:095501

http://www.springer.com/978-3-662-43623-3

Novel Optical Nanoprobes for Chemical and Biological Analysis

Chen, L.; Wang, Y.; Fu, X.; Chen, L.

2014, VIII, 100 p. 45 illus., 20 illus. in color., Softcover
ISBN: 978-3-662-43623-3